Organic Fe speciation in the Eurasian Basins of the Arctic Ocean and its relation to terrestrial DOM

Slagter, H. A.; Reader, H. E.; Rijkenberg, M. J. A.; van der Loeff, M. Rutgers; de Baar, H. J. W.; Gerringa, L. J. A.

Published in:
Marine Chemistry

DOI:
10.1016/j.marchem.2017.10.005

Publication date:
2017

Marine Chemistry 197 (2017) 11–25

Contents lists available at ScienceDirect

Marine Chemistry

journal homepage: www.elsevier.com/locate/marchem

Organic Fe speciation in the Eurasian Basins of the Arctic Ocean and its relation to terrestrial DOM

H.A. Slagter[a,*], H.E. Reader[b], M.J.A. Rijkenberg[a], M. Rutgers van der Loeff[c], H.J.W. de Baar[a,d], L.J.A. Gerringa[a,*]

[a] Department of Ocean Systems, NIOZ Royal Netherlands Institute for Sea Research and Utrecht University, Den Burg, The Netherlands
[b] National Institute for Aquatic Resources, Technical University of Denmark, Charlottenlund, Denmark
[c] Alfred Wegener Institute for Polar and Marine Research, Bremerhaven, Germany
[d] University of Groningen, Groningen, The Netherlands

ABSTRACT

The bio-essential trace metal iron (Fe) has poor inorganic solubility in seawater, and therefore dissolution is dependent on organic complexation. The Arctic Ocean is subject to strong terrestrial influences which contribute to organic solubility of Fe, particularly in the surface. These influences are subject to rapid changes in the catchments of the main contributing rivers. Here we report concentrations and binding strengths of Fe-binding organic ligands in relation to spectral properties of Dissolved Organic Matter (DOM) and concentrations of humic substances. Full-depth profiles of Fe and Fe-binding organic ligands were measured for 11 stations, good agreement to previous studies was found with ligand concentrations between 0.9 and 2.2 equivalent nM of Fe (Eq. nM Fe) at depths > 200 m. We found nutrient-like profiles of Fe in the Atlantic-influenced Nansen basin, surface enrichment in the surface over the Amundsen and Makarov basins and scavenging effects in the deep Makarov basin. A highly detailed surface transect consisting of two sections crossing the surface flow from the Siberian continental shelf to the Fram Strait, the TransPolar Drift (TPD), clearly indicates the flow path of the riverine contribution to Fe and Fe-binding organic ligands with concentrations of 0.7 to 4.4 nM and 1.6 to 4.1 Eq. nM Fe, respectively. This is on average 4.5 times higher in DFe and 1.7 times higher in Fe-binding organic ligands than outside the TPD flow path. Conditional binding strengths of ligands in the entire dataset were remarkably similar at $11.45 \leq \log K' \leq 12.63$. Increased organic Fe-binding organic ligand concentrations were evident in the Arctic Ocean surface. To better identify the organic substances responsible for Fe complexation in the Arctic Ocean, diverse analytical approaches and a standard other than Suwannee River Fulvic Acid are recommended.

1. Introduction

Iron is an essential trace element for marine primary production. It is an essential component for phytoplankton photosynthesis (Geider and La Roche, 1994) and eukaryotic DNA replication (Netz et al., 2012; Zhang, 2014). Fe concentrations in the oceans are low, and in many areas even limiting for phytoplankton growth (de Baar et al., 1990; Martin et al., 1990). Poor solubility of Fe in seawater limits inorganic Fe concentrations, depending on temperature, with lower temperatures increasing Fe solubility only in the picomolar range at seawater pH of 8.05. At room temperature the solubility of freshly precipitated Fe is ~0.08 nM, and for aged oxides it is even lower at ~0.01 nM (Millero, 1998; Liu and Millero, 2002). Dissolved Fe concentrations higher than the inorganic solubility must be facilitated by complexation with a dissolved organic ligand (Gledhill and van den Berg, 1994; Rue and Bruland, 1995). These organic ligands are diverse in nature, and relative contributions to this ligand pool are poorly understood (Gledhill and Buck, 2012; Hassler et al., 2017). Known constituents are specific Fe-binding ligands purpose-produced by bacteria called siderophores (Butler, 2005; Mawji et al., 2011). Other constituents include polysaccharide exudates (exopolysaccharides, or EPS) from bacteria and phytoplankton (Hassler et al., 2011a, 2011b), the release of cytosol contents due to viral lysis (Poorvin et al., 2011) and humic substances of terrestrial origin (Laglera et al., 2011). While the highest concentrations of Fe-binding organic ligands sometimes correlate with biological activity (Rue and Bruland, 1995; Gerringa et al., 2006, 2016), this is often not the case as described by Gerringa et al. (2015), which would then indicate non-biological or more indirect contributors

* Corresponding authors.
E-mail addresses: hans.slagter@nioz.nl (H.A. Slagter), loes.gerringa@nioz.nl (L.J.A. Gerringa).

http://dx.doi.org/10.1016/j.marchem.2017.10.005
Received 31 May 2017; Received in revised form 17 October 2017; Accepted 18 October 2017
Available online 21 October 2017
0304-4203/

to the diverse organic Fe-binding organic ligand pool.

The Arctic Ocean is a shelf-surrounded ocean and the surface waters are strongly terrestrially-influenced as described in detail by Rudels (2012). Typically, the world oceans have a low source area to basin ratio (Raiswell and Anderson, 2005), whereas the abundant Arctic shelf seas subject the Arctic Ocean to very high fluvial discharge (Stedmon et al., 2011). The introduction of river water to the Polar Surface Water (PSW) from the Siberian shelf areas is the largest terrestrial input to Eurasian Basins. This influence can be measured by a number of biogeochemical tracers of terrestrial and/or meteoric input into the Arctic Ocean. Examples are $\delta^{18}O$ in conjunction with nutrients indicating the separate inputs meteoric water and sea ice melt (Klunder et al., 2012a; Bauch et al., 2016), with the recent addition of Neodymium and other rare earth elements serving to better separate these properties in terms of the influence of the major water masses (Laukert et al., 2017). Additionally, elevated dissolved Fe (Klunder et al., 2012a) and dissolved Mn (Middag et al., 2011) indicates river water and the ^{228}Ra isotope indicates continental shelf influence (Rutgers van der Loeff et al., 1995). These tracers show surface transport along the TransPolar Drift (TPD). The TPD moves sea ice and surface water from the Siberian great rivers across the Arctic Ocean, and eventually into the northern Atlantic Ocean through Fram Strait (Gordienko and Laktionov, 1969; Gregor et al., 1998). The TPD track varies yearly dependent on the Arctic Oscillation index (Macdonald et al., 2005).

The Arctic is subject to rapid changes as a consequence of climate change (IPCC, 2014), such as the increase in river runoff (Peterson et al., 2002) and the widespread loss of permafrost (Stedmon et al., 2011; Schuur et al., 2013, 2015). Thawing permafrost has strong effects on the biogeochemistry of major rivers such as the Lena and Kolyma which flow out into the Laptev and East Siberian seas, as the thawing permafrost causes a rapid increase in organic discharge (Frey and McClelland, 2009; Vonk et al., 2012). The consequences of this discharge on DOM composition, in the shelf seas as well as in the Arctic Ocean through surface transport, are still largely unknown. The path of the TPD crosses two of three basins beyond the Siberian continental plane – the Amundsen and Makarov, separated by the Lomonosov ridge. The Nansen Basin, separated from the Amundsen basin by the Gakkel ridge, is largely uninfluenced by the TPD (Fig. 1).

Chromophoric Dissolved Organic Matter (CDOM) absorption properties can be used as tracers for riverine input (Stedmon et al., 2011) and the pool contains Fe-binding organic ligands in the form of humic substances (Laglera et al., 2007, 2011; Laglera and van den Berg, 2009). CDOM can be defined as an ocean colour property both in terms of UV–visible absorbance and UV fluorescence (Coble, 2007). With the input of humic substances, the Arctic is an area where the prime contributor to the Fe-binding organic ligand pool may be terrestrial in origin.

As techniques for the determination of Fe-binding organic ligands are essentially indirect and still non-specific with the exception of specific siderophores (Mawji et al., 2008), characterization in natural waters is largely unknown. Characterization of Fe-binding organic ligands starts with the relative contributions of different constituents to this diverse pool. In the Arctic Ocean the relative contribution of terrestrial sources is expected to be large as well as an important source for the Atlantic Ocean. Prior work in the Arctic Ocean was performed during the International Polar Year 2007 (Thuróczy et al., 2011). That study measured Fe-binding organic ligands with full depth profiles in the Nansen, Amundsen and Makarov Basins. Lower conditional binding strengths and excess ligand concentrations were found in the deep Makarov and Amundsen Basins compared to the Nansen Basin. Some surface increase of dissolved Fe-binding organic ligands was observed at stations near the TPD influence area. However, spatial resolution in this study was aimed at full depth profile comparisons between the different basins and coastal seas rather than elucidation of surface water influence. Moreover, while intersection with the TPD influence area was indicated for the Amundsen and Makarov profiles (Klunder et al., 2012a), the number of profiles sampled for ligands did not provide high lateral surface detail. In order to study the terrestrial influences in more detail, we show dissolved Fe-binding organic ligand concentrations and characteristics along two detailed transects traversing the TPD taken during the TransArcII expedition between August 15th and October 17th 2015 (FS Polarstern, PS94; Fig. 1). Additionally, spectral properties were measured to ascertain the role of CDOM, and humic substance representative concentrations were measured by way of standard additions of Fulvic acid (FA). These properties allow a first step in characterizing relative contributions to the dissolved Fe-binding organic ligand pool in the terrestrially dominated surface of the Arctic Ocean.

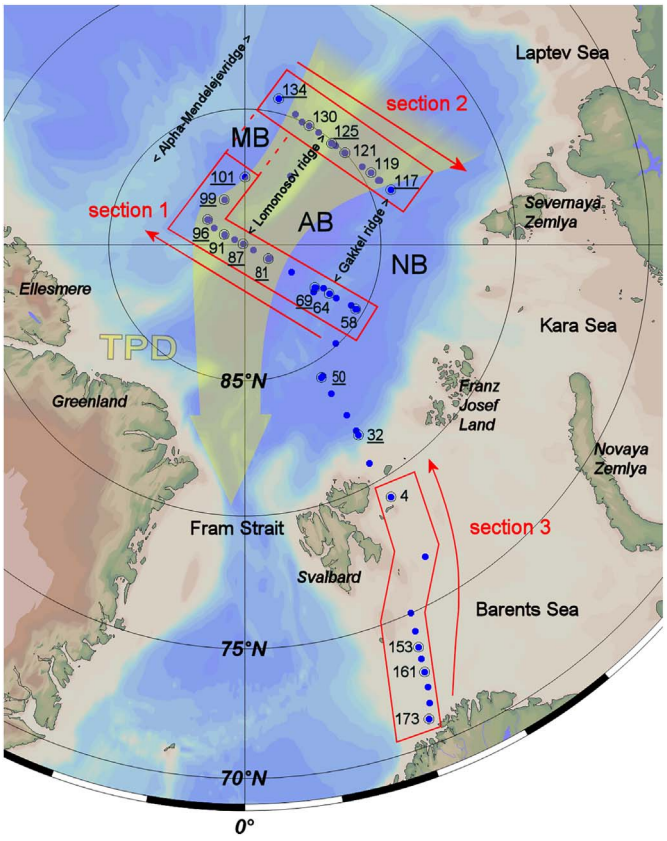

Fig. 1. Map of the study area. Stations are indicated in blue dots, stations with numbers are UCC stations, and where these are underlined basin-deep profiles were sampled. Red lines indicate the different sections with arrows indicating the direction they are plotted and/or discussed. Section 1 and 2 are combined into a single surface transect, shown in 1 section plot (Figs. 2, 5, 6). Also indicated are the Nansen Basin (NB), Amundsen Basin (AB) and Makarov Basin (MB). The broad blue arrow indicates the approximate flow path of the TPD, with boundaries based on our measurements. Map and section plots following were generated using Ocean Data View 4 (Schlitzer, 2016). (For interpretation of the references to colour in this figure legend, the reader is referred to the web version of this article.)

2. Methods

2.1. Sampling

Samples were collected with a special ultra-clean sampling system (UCC, Rijkenberg et al., 2015). Samples for the determination of dissolved Fe (DFe), dissolved Fe-binding organic ligand concentrations [L_t], CDOM and humic substances were collected through a 0.2 µm filter cartridge (Sartoban P, Sartorius) by nitrogen pressurisation of the sample bottles. All samples were taken in an ISO class 7 cleanroom environment which the UCC enters moments after arrival on deck (Rijkenberg et al., 2015). The system employed differed from the one

described by Rijkenberg et al. (2015) in that the sample bottles were constructed of polypropylene and a polyethylene cable was used (Dyneema, DSM). A standard rosette sampling system equipped with an *in-situ* fluorometer for CDOM spectral ranges (BackScat, Dr. Haardt) typically preceded UCC casts and served to target UCC bottle closure at CDOM-relevant depths. Both the UCC and rosette frame employed a set of Conductivity Temperature Depth (CTD) sensors for the calculation of practical salinity, potential temperature and sampling depths. Nutrient samples were taken from both systems and analysed after Murphy and Riley (1962, phosphate), Strickland and Parsons (1972, silicate) and Grasshoff (1983, nitrate) using a TRAACS 800 autoanalyser (Technicon).

Two sections in the central Arctic Ocean cross the TPD (Fig. 1), encompassing 29 rosette stations and 13 UCC stations. Furthermore, a third section is defined from the Norwegian coast passing Svalbard into the Nansen Basin, encompassing 16 rosette stations and 6 UCC stations. Full depth profiles for [L_t] and all CDOM spectral properties were sampled at UCC stations 32, 50, 69, 81, 87, 96, 99, 101, 117, 125 and 134. Other UCC stations were limited to 200 m depth and humic substances were measured down to 150 m. Maps and section plots are generated using Ocean Data View 4 (Schlitzer, 2016). Stations 32 to 134 were under full ice cover, while stations 4 and 153 to 173 were in open water (Schauer, 2016).

2.2. Materials handling

Chemical preparation and equipment cleaning took place in an ISO class 7 ultra-clean (UC) laboratory environment (Interflow) with ISO class 5 workspaces. When outside the UC environment, sample handling took place inside laminar flow hoods (ISO class 5, Interflow and AirClean systems). All material rinsing and chemical preparation was performed using ultrapure water (18.2 MΩ cm, Milli-Q Element, Merck Millipore), further referred to as MQ. Sample and solution bottles for trace metal analysis were low density polyethylene (LDPE) and fluorinated ethylene propylene (FEP) bottles (both Nalgene) cleaned with hydrochloric acid (HCl) after GEOTRACES protocols (Cuttler et al., 2010). A sub-boiling Teflon distillation apparatus (Savillex) was used twice (2 × D) to purify HNO_3 and methanol for cleaning and chemical preparation.

Buffer solutions used for analysis of Fe-binding organic ligand characteristics were cleaned by equilibration with a manganese dioxide (MnO_2) suspension and subsequent filtration after van den Berg and Kramer (1979). In short, the MnO_2 suspension was prepared by combining a 0.03 M $MnCl_2$ solution and a 0.02 M $KMnO_4$ solution, subsequent centrifugation in 50 mL tubes (VWR) at ~4000 rpm for 5 min using an Eppendorf 5810R centrifuge. The precipitate was resuspended in MQ and the centrifugation process was performed 3 times. Cleaning of solutions was performed twice, using a 100 μM final concentration of MnO_2 left to equilibrate in motion for ~8 h to overnight and finally removed using HCl (1 M) cleaned 0.2 μm polycarbonate filters (Whatman) in a polysulfone filter tower (Nalgene, also 1 M HCl cleaned; van den Berg, 2006).

2.3. Determination of DFe concentrations

Samples for DFe were collected from the Fe-binding organic ligand sample bottles at the time of voltammetric analysis and acidified with 2‰ v/v 12 M trace metal grade HCl (Seastar Chemicals). DFe concentrations (expressed in nM) were then measured using an automated Flow Injection Analysis system the same day (Klunder et al., 2011). The sample was transferred onto an iminodiacetic acid (IDA) column, binding only transition metals and serving to concentrate and desalt the retentate. The column was subsequently washed with MQ and eluted with HCl (0.4 M, Merck Suprapur). Luminol (0.6 mM, Aldrich), hydrogen peroxide (0.6 M, Merck Suprapur) and dilute ammonia (0.96 M, Merck Suprapur) are then mixed in. Iron catalyses the oxidation of luminol by hydrogen peroxide, producing blue light in correlation to the amount of catalyst present (Obata et al., 1993). The response of a photon counter is calibrated with a series of Fe standard additions (ICP standard, Fluka, Sigma-Aldrich). Samples are analysed in triplicate and reported with a standard deviation of the mean (SD), which averages 2.9%. Blanks averaged 0.017 ± 0.02 nM during the expedition. The detection limit of the system, defined as 3·SD of daily blanks was 0.06 nM. Quality control for the system was maintained by daily measurement of lab standards and regular measurement of certified reference material (Rijkenberg, unpublished results).

2.4. Fe-binding organic ligands

Total Fe-binding organic ligand concentration [L_t], expressed as equivalent nM of Fe (Eq. nM Fe), and the conditional binding strength (K′) with respect to inorganic Fe (Fe′), further reported as the base-10 logarithm (LogK′) were measured with Competitive Ligand Exchange–Adsorptive Cathodic Stripping Voltammetry (CLE-AdCSV), using 2-(2-thiazolylazo)-*p*-cresol (TAC) after Croot and Johansson (2000). Due to the labour-intensive character of the measurements, samples for Fe-binding organic ligand characterization were typically frozen after sampling and processed in order on a schedule independent from the sampling regimen. A natural sample was left to equilibrate with the competitive ligand TAC (Alfa Aesar) in the presence of a mixed boric acid-ammonia buffer (1 M, pH 8.05, Merck) and increasing standard additions of Fe(III) from 0 to 8 nM. The resulting titration with Fe was analysed for $Fe(TAC)_2$ concentration using differential pulse voltammetry. A TAC solution of 0.02 M was prepared in 3 × D-methanol, Fe standards (1 and $3 \cdot 10^{-6}$ M) were prepared in MQ from a 1000 ppm ICP stock solution (Fluka) acidified using 2 × D-HNO_3. The voltammetric apparatus consisted of a 663 VA stand (Metrohm) equipped with a Hg drop multimode electrode with silanized capillary, double-junction Ag/AgCl reference electrode (KCl 3 M) and glassy carbon auxiliary electrode in a polytetrafluoroethylene (PTFE) cell (all Metrohm), control hardware (μAutolab III, Metrohm Autolab B.V.) and a consumer laptop PC running Nova 1.9 (Metrohm Autolab B.V.). N_2 was used for purging and Hg drop formation. Interference from ship motion and vibration was minimized by suspending the VA stand in elastic bands. Any electrical interference was minimized using a consumer inline peak filter and an uninterruptible power supply with sinewave converter (Fortress 750, Best Power). Analysis was performed using a slightly altered version of the procedure used by Croot and Johansson (2000): Purging for 180 s, no conditioning, deposition for 140 s at −0.4 V, a 5-second equilibration followed by a differential pulse scan from −0.4 to −0.9 V. The influence of high frequency vibrations from the ship's drivetrain was minimized by an increased scan rate of 39 mV s^{-1} (0.05 s interval and 0.004 s modulation time). 30 mL PTFE cups (Savillex) were used to equilibrate 10 mL subsamples from a mix of natural sample, buffer (5 mM final concentration) and TAC (10 μM final concentration) with discrete Fe(III) additions of 0 (twice), 0.2, 0.4, 0.6, 0.8, 1.0, 1.2, 1.5, 2.0, 2.5, 3.0, 4.0, 6.0 and 8.0 (twice) nM. Equilibration lasted a minimum of 8 h to overnight.

Titrations were analysed for natural ligand concentration and binding strength by a non-linear fit of the Langmuir model after Gerringa et al. (2014) using R (R Development Core Team, 2008). Where it was possible to resolve 2 ligands, these were also calculated using the same method with the strongest class designated L_1 and the weaker class designated as L_2 (Gledhill and Buck, 2012). Inorganic Fe′ [Fe′] is defined as the product of [Fe^{3+}] and the inorganic side reaction coefficient ($\alpha_{Fe'}$), for which a value of 10^{10} was used after Liu and Millero (2002). The excess ligand concentration [L′] is the available binding capacity, *i.e.* the amount of unbound organic Fe-binding sites, as is defined as in Eq. (1):

$$[L'] = \frac{[L_t]}{1 + K' \bullet [Fe^{3+}]} \quad (1)$$

[L′] approaches 0 where [L_t] is insufficient to bind further Fe. [Fe^{3+}] and [L′] were determined from DFe and Eq. (1) by iterative calculations of the Fe speciation equilibrium with Newton's algorithm

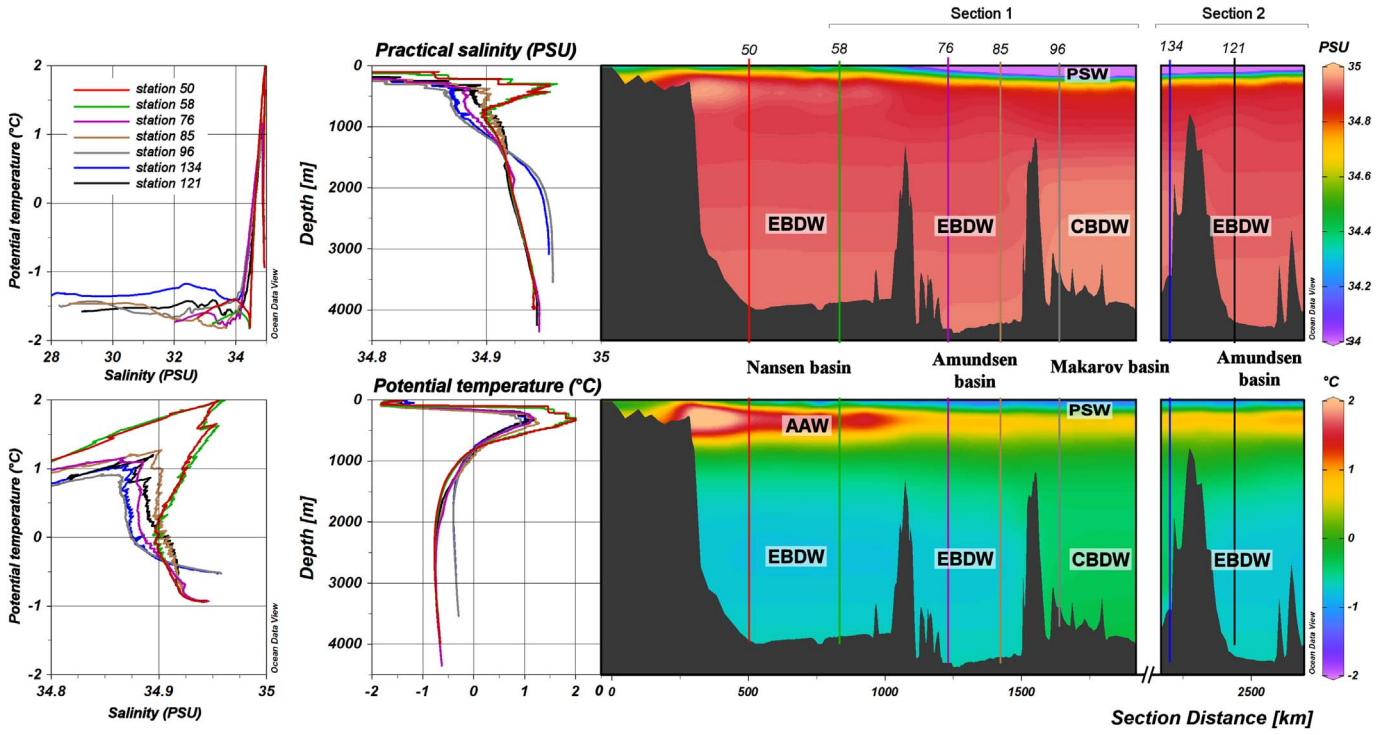

Fig. 2. TS profiles and section plots of the deep parts of the study area, from the shelf at Station 4 to the end of Section 2 at Station 134. The left side property-property plots show the relation between potential temperature and salinity (T-S, left), as well as depth profiles attached to the section plots (middle), for Stations 40, 58, 76, 85, 96, 134 and 121. Of the T-S plots on the left, the top shows the entire salinity range and the bottom plot details small-scale salinity variations to help characterize water masses after Rudels (2010, 2012). Polar Surface Water (PSW), Eurasian Basin Deep Water (EBDW), Canadian Basin Deep Water (CBDW) and Arctic Atlantic Water (AAW) are indicated in the practical salinity and potential temperature sections.

(Press et al., 2007), using an R implementation of the method described by Gerringa et al. (2014). The ratio $[L_t]$/DFe reflects the surplus of Fe-binding organic ligands. Ratios > 1 indicate that there is sufficient binding capacity to explain DFe, whereas a ratio between 0 and 1 would indicate a lack of binding capacity (Thuróczy et al., 2010). The reactivity of the ligands α_{FeL} is the product of K′ and [L′] (Ringbom and Still, 1972; Gledhill and Gerringa, 2017), expressed as the base-10 logarithm with respect to Fe′, further referred to as $Log\alpha_{FeL}$.

2.5. Humic substances

The concentration of humic substances [HS] was measured using cathodic stripping voltammetry after Laglera et al. (2007). Samples were buffered with a boric acid-ammonia solution (1 M, pH 8.05, Merck) and saturated with Fe(III) by a 30 nM addition from a $3 \cdot 10^{-6}$ M standard prepared from a 1000 ppm ICP stock (Fluka). To increase the current signal of the dissociating Fe-humic complex at the electrode $KBrO_2$ (13 μM final concentration) served as oxidizer. Standard additions of fulvic acid (Suwannee River Fulvic Acid Standard I, International Humic Substances Society (IHSS), St. Paul, USA, further referred to as FA) of 0.1 to 0.4 mg/L were used as a measure of equivalent quantification. Therefore [HS] is expressed in the equivalent mg/L of fulvic acid (Eq. mg/L FA) and is specific to the standard used. Expression in a molar concentration would require further information on the FA standard than is currently available (Laglera et al., 2007). Analysis was performed with the same voltammetric equipment as used for CLE-AdCSV. The procedure employed a 180 s purge followed by a 90 s deposition period at − 0.1 V and a linear current sweep from − 0.1 to − 1.1 V at a scan rate of 100 $mV \cdot s^{-1}$ (0.05 s interval).

2.6. Dissolved organic matter

For the characterization of CDOM, absorbance spectra between 250 and 1000 nm, at 1 nm resolution, were recorded for each sample in a quartz cell with a 1 cm path length (SUPRASIL®, Hellma Analytics) using a Spectramax M2 multimode spectrophotometer (Molecular Devices). Daily measurements of MQ were used as blanks, the spectra of these were subtracted from the data as a baseline correction. A further baseline correction was performed by subtracting the mean absorbance between 450 and 500 nm in order to correct refractive index differences between seawater and the MQ blanks. Extremely low values of absorbance at longer wavelengths, nearing the limit of detection, dictated the use of the 450–500 nm window for that correction. The absorbance in RFU (A_λ) was converted into absorption coefficients (a_λ, m^{-1}) using path length (l, m) and ln(10) according to Stedmon et al. (2000):

$$a_\lambda = 2.303 \frac{A_\lambda}{l} \quad (2)$$

Spectral slopes for the intervals 275–295 nm (S_{275}) and 350–400 nm (S_{350}) were calculated by linear fitting to the ln(a) spectrum using R. Absorption values were recorded at wavelengths of 254 nm (a_{254}) and 300 nm (a_{300}) as indicators of complex organics (Helms et al., 2008). The fluorescent fraction of DOM (FDOM) was analysed using UV fluorescence spectrophotometry (Mopper and Schultz, 1993). Emission spectra were recorded between 360 and 540 nm with an interval of 1 nm at an excitation wavelength of 250 nm using the same equipment as above. Emission at 450 nm using this excitation wavelength ($F_{250/450}$) was taken as a measure of humic-like FDOM (Coble et al., 1998; Coble, 2007). Daily measurements of a 1 mg/L quinine sulfate (QS) standard (Alpha Aesar, dissolved in MQ with 0.1 M H_2SO_4) served as an equivalent reference for expression of FDOM concentrations. FDOM measurements are thus expressed as equivalents of 1 ppb QS emission at 450 nm using 250 nm excitation, referred to as quinine sulfate units (QSU; Mopper and Schultz, 1993).

3. Results

3.1. Hydrography and nutrients

Fig. 2 shows temperature and salinity data with emphasis on the deep

parts of the study area. Polar Surface Water (PSW), discussed in more detail in the next paragraph, is characterized by salinities under 34.5 and temperatures < 0 °C. Atlantic Water enters the Arctic Ocean from Fram Strait along the Eurasian shelf seas. This becomes Arctic Atlantic Water (AAW) in the upper layer between 200 and 900 m, characterized by the highest potential temperatures of > 0 °C (Rudels, 2010). Below the AAW, low temperature Polar Deep Water (PDW) is found, characterized by potential temperatures < 0 °C and salinities > 34.9. A distinction is made between Eurasian Basin Deep Water (EBDW) in the Nansen and Amundsen Basins where potential temperatures down to −1 °C are found, and Canadian Basin Deep Water (CBDW) characterized by a higher potential temperature maximum of −0.5 °C (Rudels, 2010, 2012), which is also found in the Makarov basin (Fig. 2). An intermediate layer with temperatures of −0.5–0 °C identified by Rudels (2010) is not differentiated from PDW in this study.

The surface of the Arctic Ocean is subject to sea ice melt and terrestrial runoff, giving the PSW relatively low salinities and temperatures. Sections 1 and 2 are connected and presented as one transect (Figs. 1, 3). All stations in this transect were under full sea-ice cover. This transect is limited to 200 m depth and will be further referred to as the surface transect. Temperature in the upper 100 m was relatively constant (mean −1.54 °C, SD = 0.21, N = 278) with a small protrusion of warmer water between Station 81 and 121 in the middle of the surface transect (ΔT ≈ 0.25 °C; Fig. 3a, contours). Between 100 and 200 m temperature changed with depth from −1.25 to ~0 °C (mean −0.04 °C, SD = 0.93, N = 123), marking the transition to the upper boundary of AAW. For Stations 58 to 64 of Section 1 the warmer layer occurred further upward in the water column, nearer to 100 m depth and with a mean temperature of 1.58 °C between 200 and 400 m depth. This area correlates with the inflow of Atlantic water (Fig. 2). Rudels (2010) describes a Polar Mixed Layer (PML), which is limited to the upper 50 m and has salinities < 34 PSU. We will use this PML depth of 50 m as a constraint to report mixed layer values inside our surface transect. Surface hydrography is discussed in terms of density anomaly (σ_θ), for which salinity is the dominating factor in the PSW (Fig. 3a). A decrease of σ_θ (< 25 kg m^{-3}) was observed in the surface transect above 50 m between Stations 81 and 119, pressing the halocline downward. This part of the surface transect encompasses our samples over half the Amundsen Basin and all our samples over the Makarov Basin. Outside this area (Stations 58 to 76 and 115 to 119), σ_θ was 26.8 kg m^{-3} with values up to 27.7 kg m^{-3} (depth < 50 m (PML), SD = 0.6 kg m^{-3}, N = 63). In contrast, in the low-σ_θ region σ_θ was 24.3 kg m^{-3} with values as low as 21.8 kg m^{-3} (< 50 m, SD = 1.5 kg m^{-3}, N = 98).

Elevated phosphate concentrations extended from ≥100 m depth to the PML in the low-σ_θ region (Fig. 3b, colours). Phosphate concentrations in the low-σ_θ region were 0.65 μM (< 50 m, stations as above, SD = 0.16 μM, N = 117) against a mean background of 0.38 μM (< 50 m, stations outside the low-σ_θ region as above, SD = 0.08 μM, N = 58). The surface minimum phosphate concentration between Stations 58 to 76 of 0.38 μM connected to a subsurface minimum of similar values, with higher concentrations of 0.65 μM at Stations 81 and 85 above that at 25 m (Fig. 3b). Nitrate concentrations show a similar deepening minimum towards station 87 (Fig. 3b, contours). However, surface concentrations stayed ≤2.5 μM above 25 m in the low-σ_θ region. Horizontally along our surface transect nitrate concentrations mostly increase evenly with depth to ≥7.5 μM from 100 m depth downwards, only disturbed by the subduction between Stations 76 and 87 (Fig. 3b). Average silicate concentrations were higher in the low-σ_θ region at 11.13 μM (depth < 50 m, stations as above, SD = 3.42 μM, N = 117), outside of the low-σ_θ region concentrations were 2.85 μM (< 50 m, SD = 1.35 μM, N = 58; Fig. 3c). Given the nutrient and salinity-derived density character of the low- σ_θ region, a strong influence from the Chukchi Sea with a Pacific origin is indicated here (Cooper et al., 1997).

A surface increase of CDOM fluorescence data from the *in-situ* sensor on the rosette sampler was observed between Stations 81 and 101 in Section 1 and between Stations 118 and 132 in Section 2 (Fig. 3d). Measurements by this sensor were 0.59 arbitrary units (a.u.) at these stations (< 50 m, SD = 0.07 a.u., N = 53) against a background of 0.36 a.u. (< 50 m, SD = 0.07 a.u., N = 42). Based on this known tracer for the terrestrial influence that defines the TPD (Amon et al., 2003; Coble, 2007), the TPD influence area during our study was operationally constrained as those records where *in-situ* CDOM fluorescence was 0.5 a.u. or higher. At Station 134 there were no measurements due to a break in rosette sampler deployment. Based on the strong agreement with CDOM absorption coefficients (Section 3.3) this station was judged as outside the TPD.

3.2. Deep water properties of DFe and Fe-binding organic ligands

Below 200 m in the Nansen Basin the DFe profiles showed a subsurface maximum near the continental shelf (0.76 nM at 385 m, Station 32), and otherwise settled at a more or less constant value of 0.50 nM at depth (> 200 m, SD = 0.14 nM, N = 13). A deep maximum was observed near the continental shelf (0.77 nM at 2556 m, Station 32). In the Amundsen Basin there was surface enrichment of DFe with a subsurface minimum reached at < 200 m depth. Deep values were constant at 0.53 nM (> 200 m, SD = 0.04 nM, N = 34) for the Section 1 stations in the Amundsen Basin (64, 69, 81 and 87) and 0.39 nM (> 200 m, SD = 0.06 nM, N = 12) for the Section 2 stations (117 and 125), the latter had bottom minima of 0.23 nM at 4119 m and 0.32 nM at 3633 m, respectively. In the Makarov Basin the surface characteristics of DFe were similar to Amundsen Basin. However, here there was a small decrease of concentrations with depth from subsurface minima of 0.20–0.31 nM (Station 101 at 363 m, Station 99 at 486 m) to deep minima of 0.10–0.19 nM (Station 134 at 2939 m, Station 99 at 3453 m).

In the Nansen Basin below 200 m depth [L_t] was relatively constant with an average of 1.28 Eq. nM Fe (> 200 m, SD = 0.16 Eq. nM Fe, N = 12), with the exception of a local deep high concentration of 2.22 Eq. nM Fe at 2940 m (Station 50, Fig. 4). In the Amundsen Basin [L_t] was 1.33 Eq. nM Fe on average at > 200 m depth (SD = 0.25 Eq. nM Fe, N = 29). Notable elevated concentrations were found at 1962 m at Station 87 (2.02 Eq. nM Fe) and at 980 m at Station 81 (1.83 Eq. nM Fe). Maxima at ~1000 m occurred at Stations 81, 101 and 117 in the Amundsen Basin. In the Makarov Basin [L_t] depth profiles were similar to those in the Amundsen Basin, but with gradual increases with depth from 1000 m onwards at Stations 96, 101 and 134. [L_t]/DFe ratios at > 200 m depth (Fig. 5) settled at a low value of 2–3 in the Nansen basin with a minimum approaching 1 in the upper AAW layer at station 32 (Nansen basin) and gradually declined to another minimum at 2500 m depth. At Station 50 a deeper occurrence of higher ratios towards the surface also coincides with the AAW layer. In the Amundsen Basin the [L_t]/DFe ratios were consistently varying around 3 with no discernible trend, with variation dictated by changes in [L_t]. In contrast to the Nansen and Amundsen basins, [L_t]/DFe ratios in the Makarov Basin (Stations 96, 99, 101 and 134) increased with depth. Deep maxima here were 7.1 (Station 96, 3292 m), 4.9 (Station 99, 3453 m), 9.4 (Station 101, 3702 m) and 11.8 (Station 134, 3010 m).

Table 1 summarizes DFe and Fe-binding organic ligand data for all profiles at full depth stations in the Arctic Ocean. The most pronounced variability in DFe, [L_t], [L′], and ratio [L_t]/DFe was observed in the surface (≤200 m depth). In most cases the most extreme values and highest standard deviations were found in this layer, which is described in a higher spatial resolution in the next section. The AAW layer did not substantially differ from the PDW or entire > 200 m depth layers in terms of DFe and Fe-binding organic ligand properties, therefore this layer is not separately shown in Table 1. The Nansen and Amundsen basins did not differ significantly below 200 m depth, with respectively a mean DFe of 0.50 and 0.48 nM (SD = 0.13 and 0.09 nM), a mean [L_t] of 1.35 and 1.37 Eq. nM Fe (SD = 0.30 and 0.28 Eq. nM Fe) and a mean [L′] of 0.85 and 0.89 Eq. nM Fe (SD = 0.31 and 0.25 Eq. nM Fe). The mean [L_t]/DFe ratio was 2.9 for both Nansen and Amundsen basins (SD = 0.9 and 0.6). Mean DFe in the Makarov basin differed significantly from the Nansen and Amundsen basins at 0.23 nM (SD = 0.07). Mean [L_t] and [L′] were only

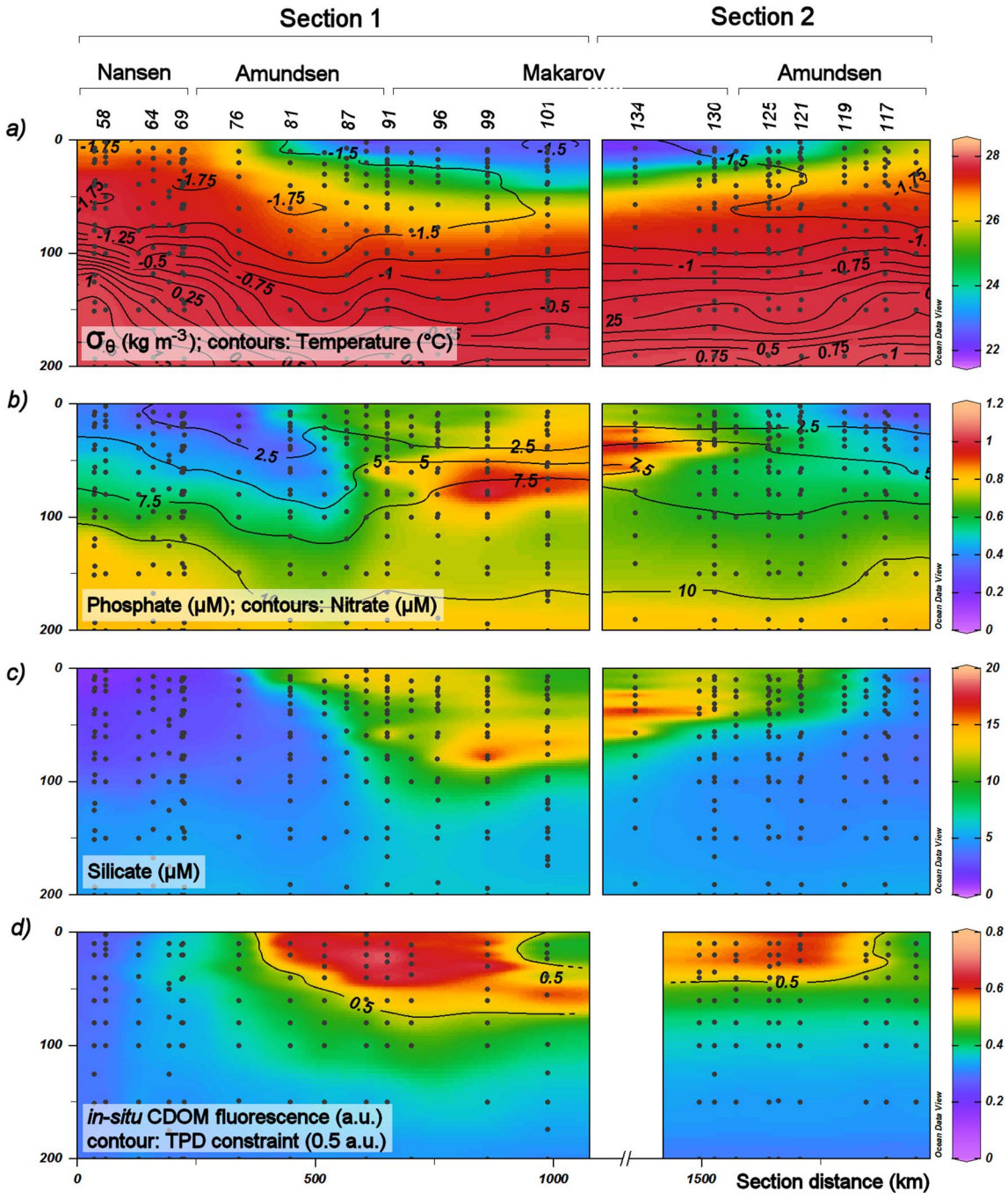

Fig. 3. Hydrographical, nutrient and *in-situ* CDOM fluorescence properties for the upper 200 m of the water column along sections 1 (Stations 58 to 101) and 2 (Stations 117 to 134). a) Potential density σ_θ expressed in kg·m^{-3} (colour scale) and potential temperature in degrees Celsius (contours), b) phosphate concentration in µM (colour scale) and nitrate concentration in µM (contours), c) silicate concentration in µM, and d) *in situ* CDOM fluorescence measurements as registered for discrete bottle closure depths in arbitrary units, the contour indicates the 0.5 a.u. constraining value used to discriminate between records inside and outside the TPD. Stations and corresponding sections are indicated above the image. (For interpretation of the references to colour in this figure legend, the reader is referred to the web version of this article.)

slightly and not significantly lower than in the Nansen and Amundsen basins at 1.20 Eq. nM Fe (SD = 0.21) and 0.96 Eq. nM Fe (SD = 0.23), respectively. As a result, the mean [L_t]/DFe ratio was also different at 5.5 (SD = 2.4). Logα_{FeL} was slightly but not significantly higher in the Makarov Basin compared to the Nansen and Amundsen basins at 3.07 ± 0.32 *versus* 2.95 ± 0.22 and 2.83 ± 0.20, respectively (Table 1). Mean LogK′ values are near uniform across the entire > 200 m dataset at 11.99 mol^{-1} (SD = 0.26, N = 63, range 11.50 ≤ LogK′ ≤ 12.62 mol^{-1}). Determination of a second ligand class was possible for 27 measurements out of 63 samples at depths > 200 m (Table 2). Where these were found, the L_1 class had a mean concentration of 0.62 Eq. nM Fe (0.16 ≤ [L_1] ≤ 0.95, SD = 0.20 Eq. nM Fe) and the L_2 class had a mean concentration of 1.28 Eq. nM Fe (0.70 ≤ [L_2] ≤ 2.70, SD = 0.49 Eq. nM Fe). LogK′ for the L_1 class was a mean 13.14 mol^{-1}, LogK′ for the L_2 class was a mean 11.16 mol^{-1} (SD = 0.61 and 0.17 mol^{-1}, respectively). These concentrations and corresponding LogK′ values did not differ significantly between basins.

3.3. Surface properties of DFe, Fe-binding organic ligands, CDOM and humic substances

In the Nansen Basin, DFe was very low in the upper 200 m, at

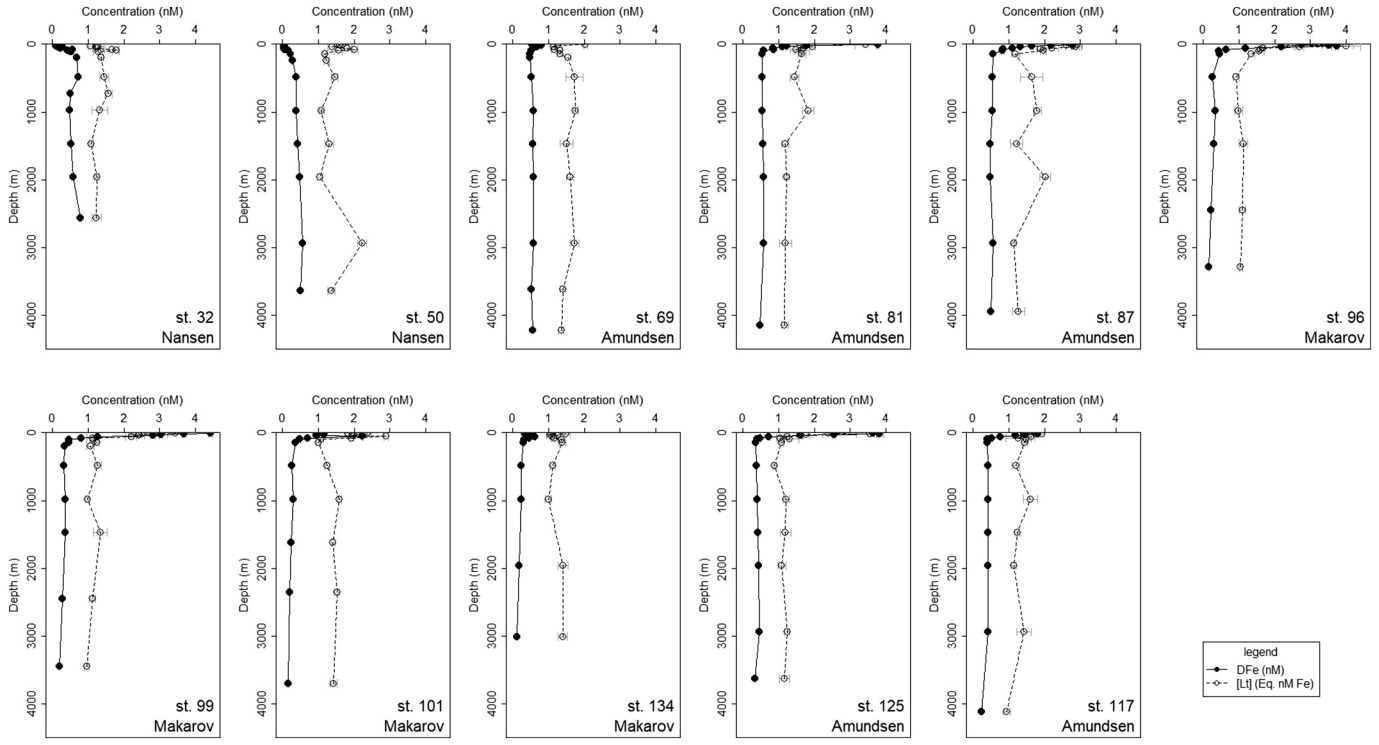

Fig. 4. Depth profiles of dissolved Fe concentrations (DFe) in nM (solid lines with filled circles) and Fe binding organic ligand concentrations ($[L_t]$) in equivalent nM of Fe (dashed lines with open diamonds). Station numbers are indicated as well as the basins these reside in. Error bars indicate standard deviations for multiple measurements (N = 2 or 3) for DFe and the standard error of the Langmuir fit for $[L_t]$. Where error bars are not visible these fall inside of the symbols.

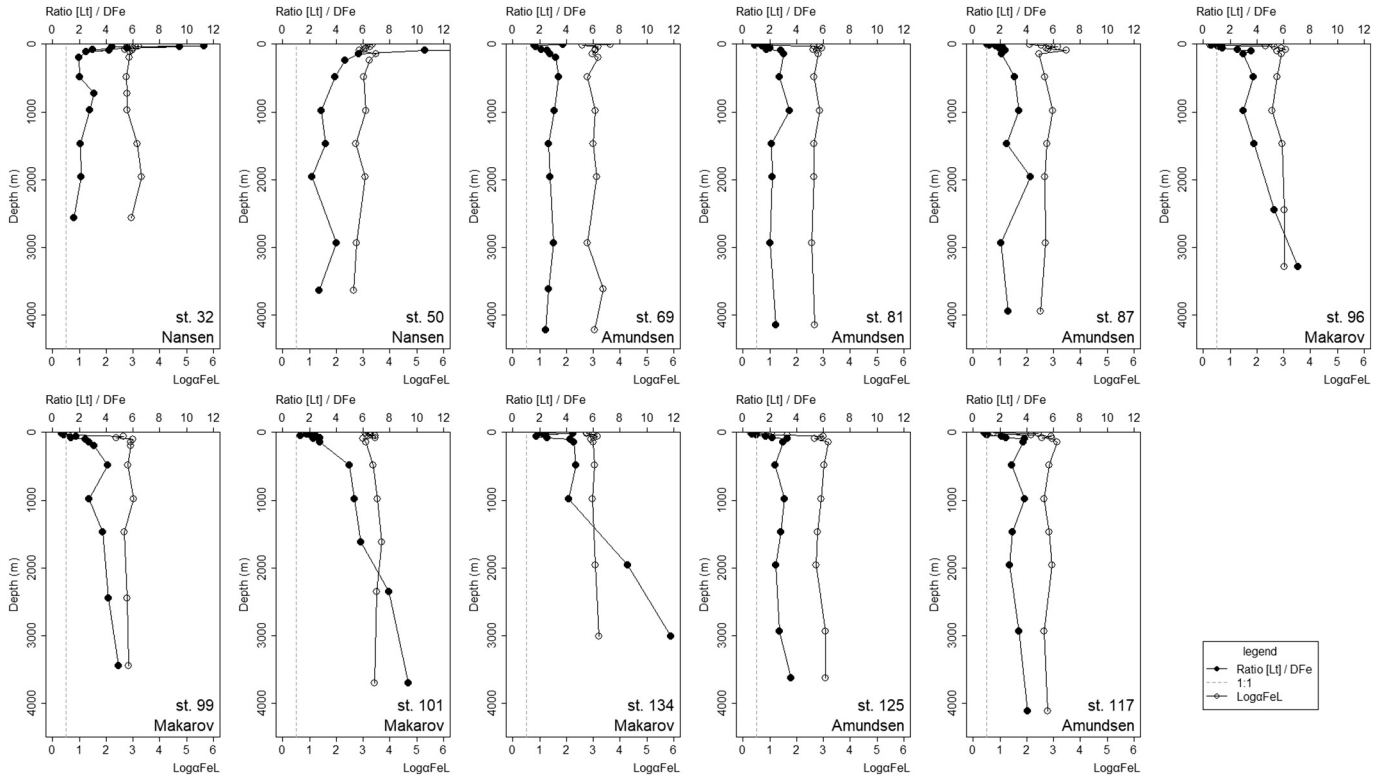

Fig. 5. Depth profiles of the ratio between $[L_t]$ and DFe (top axis, filled circles) as well as $Log\alpha_{FeL}$ (bottom axis, open circles) for the same stations as in Fig. 4. The dashed line indicates a ratio of 1.

Table 1
Mean values with standard deviations, number of records and extreme values for Fe speciation at full depth stations in the Arctic Ocean (St. 32, 50, 69, 81, 87, 96, 99, 101, 117, 125 and 134).

		DFe (nM)	[L_t] (Eq. nM Fe)	LogK′ (mol^{-1})	Logα_{FeL}	[L′] (Eq. nM Fe)	[Lt]/DFe (ratio)
Surface	Average	0.99	1.75	12.03	2.60	0.75	4.6
(≤ 200 m)	SD	1.01	0.68	0.26	0.84	0.47	8.9
	N	116	87	87	87	87	87
	min	0.03	1.00	11.45	0.26	< 0.01	0.6
	max	4.42	4.01	12.63	3.64	1.95	53.5
Deep Nansen Basin	Average	0.50	1.35	12.04	2.95	0.85	2.9
(> 200 m)	SD	0.13	0.30	0.31	0.22	0.31	0.9
St. 32 & 50	N	27	13	13	13	13	13
	min	0.26	1.04	11.54	2.64	0.46	1.6
	max	0.77	2.22	12.50	3.32	1.66	4.7
Deep Amundsen Basin	Average	0.48	1.37	11.90	2.83	0.89	2.9
(> 200 m)	SD	0.09	0.28	0.22	0.20	0.25	0.6
St. 69, 81, 87, 117 & 125	N	66	31	31	31	31	31
	min	0.23	0.89	11.50	2.52	0.52	2.0
	max	0.63	2.02	12.42	3.36	1.55	4.3
Deep Makarov Basin	Average	0.23	1.20	12.10	3.07	0.96	5.5
(> 200 m)	SD	0.07	0.21	0.25	0.32	0.23	2.4
St. 96, 99, 101 & 134	N	52	19	19	19	19	19
	min	0.10	0.92	11.67	2.56	0.62	2.7
	max	0.36	1.58	12.62	3.69	1.32	11.8

Table 2
2-Ligand determination for full depth profiles in Sections 1 and 2 (Stations 32, 50, 69, 81, 87, 96, 99, 101, 117, 125 and 134).

		[L_t] 1 (Eq. nM Fe)	LogK′ 1 (mol^{-1})	Logα_{FeL} 1	[L′] 1 (Eq. nM Fe)	[L_t] 2 (Eq. nM Fe)	LogK′ 2 (mol^{-1})	Logα_{FeL} 2	[L′] 2 (Eq. nM Fe)
All	Average	0.62	13.14	3.41	0.29	1.28	11.16	2.23	1.23
> 200 m	SD	0.20	0.61	0.81	0.21	0.49	0.17	0.22	0.48
	N	27	27	27	27	27	27	27	27
	Min	0.16	12.30	1.77	< 0.01	0.70	10.61	1.59	0.67
	max	0.95	14.59	5.09	0.79	2.70	11.38	2.64	2.60
Nansen Basin	Average	0.64	12.85	3.18	0.25	1.13	11.19	2.21	1.08
St. 32 & 50	SD	0.18	0.37	0.30	0.14	0.25	0.12	0.22	0.24
	N	5	5	5	5	5	5	5	5
	min	0.46	12.30	2.81	0.09	0.71	11.06	1.90	0.69
	max	0.88	13.34	3.50	0.40	1.38	11.34	2.47	1.34
Amundsen Basin	Average	0.62	13.05	3.29	0.21	1.34	11.18	2.26	1.28
St. 69, 81, 87, 117 &	SD	0.16	0.57	0.67	0.11	0.48	0.11	0.14	0.47
125	N	12	12	12	12	12	12	12	12
	min	0.41	12.44	2.47	0.04	0.70	11.01	2.06	0.67
	max	0.91	14.59	4.98	0.36	2.34	11.36	2.52	2.32
Makarov Basin	Average	0.61	13.38	3.68	0.41	1.28	11.14	2.20	1.26
St. 96, 99, 101 & 134	SD	0.26	0.69	1.10	0.27	0.61	0.24	0.31	0.59
	N	10	10	10	10	10	10	10	10
	min	0.16	12.54	1.77	< 0.01	0.73	10.61	1.59	0.73
	max	0.95	14.39	5.09	0.79	2.70	11.38	2.64	2.60

0.21 nM (SD = 0.20, N = 18, Stations 32, 40 and 50), with a minimum of 0.03 nM at 20 m depth over the middle of the basin (Station 50) and a maximum of 0.69 nM at 198 m near the shelf (Station 32). Horizontal variation of Fe speciation and CDOM properties was large and similar between all properties in the surface transect (Fig. 6). In strong agreement with the *in-situ* CDOM fluorescence (Fig. 3d) and our TPD definition of ≥ 0.5 a.u., DFe (Fig. 6a) in Section 1 increased sharply between Stations 81 and 99 with the highest concentrations in the upper 10–40 m (*e.g.* 4.42 nM at 8 m depth, Station 99) against an average background of 0.58 ± 0.38 nM (outside the TPD). Similarly, DFe was high between Stations 119 and 130 inside the TPD in Section 2 (*e.g.* 4.35 nM at 7 m depth, Station 121).

Between Stations 81 and 99 [L_t] (Fig. 6b) also increased, with the highest concentration of 4.13 Eq. nM Fe at 39.9 m depth (Station 91). To a lesser extent, [L_t] also increased between Stations 119 and 130, with the highest concentration in the area corresponding with TPD constraints of 3.55 Eq. nM Fe at 16.7 m depth at station 125. Additionally, at 95.6 m depth at Station 119 an [L_t] of 3.91 Eq. nM Fe (SE = 0.185 Eq. nM Fe) is recorded outside the TPD constraints. Similarly, a singular high [L_t] of 2.44 Eq. nM Fe (SE = 0.323 Eq. nM Fe) is found at 141.3 m depth at Station 91. The outside-TPD background [L_t] using the same constraints is 1.51 Eq. nM Fe (SD = 0.48 Eq. nM Fe, N = 74; Table 3). In the Nansen Basin [L_t]/DFe ratios (Figs. 5, 6c) at the surface (< 200 m depth) are high, whereas surface [L_t]/DFe ratios in the Amundsen and Makarov Basins are low, in cases between 0 and 1 in the PML in the surface transect. Ratios of [L_t]/DFe shown in Fig. 6c are very low inside the TPD, with values between 0 and 1, especially in Section 2 between Stations 117 and 130. The outliers reported for [L_t] results in high ratios (7.9 at 141.3 m, Station 91; 8.9 at 95.6 m, Station 119) which are also higher than the outside-TPD background of 2.7 (SD = 1.4, N = 74; Table 3). The average Logα_{FeL} inside the TPD was notably lower at 1.66 against 2.89 outside the TPD. However, variability of Logα_{FeL} inside the TPD was high leading to a large SD of 1.17 (N = 35), lowering significance of the difference with values outside the TPD (SD = 0.53, N = 74; Table 3).

LogK′ in the surface transect reprises the uniformity observed in deep water at 12.08 mol^{-1} (SD = 0.30, N = 109, range 11.40 ≤ LogK′ ≤ 12.91 mol^{-1}). Two ligand classes could be determined for 32 out of 86 samples at ≤ 200 m depth (Table 4). However, the ability to

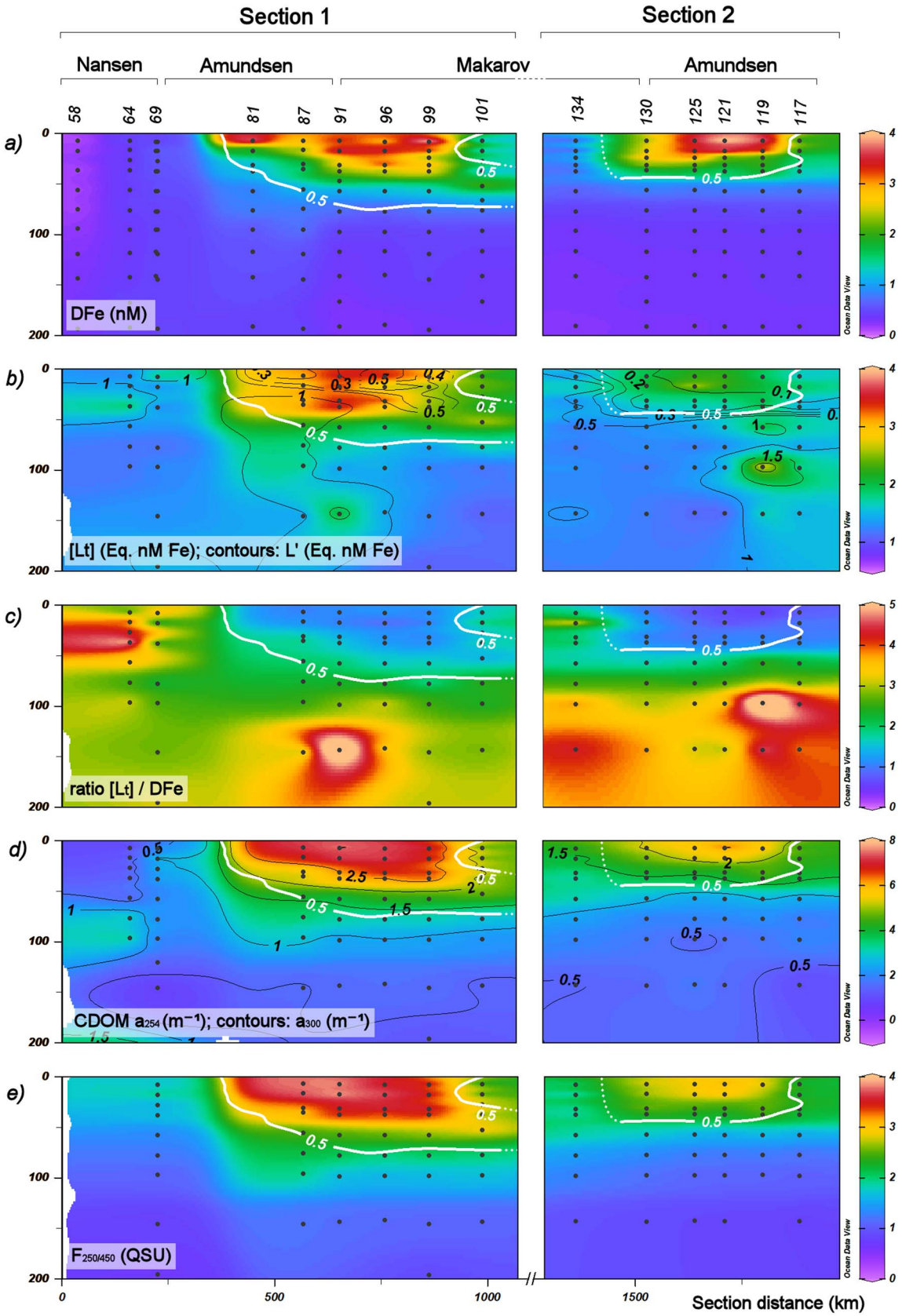

Fig. 6. DFe, [Lt], and CDOM properties for the upper 200 m of the water column along Sections 1 and 2. a) DFe in nM, b) [L_t] (colour scale) and [L′] (contours) in equivalent nM of Fe, c) the ratio between [L_t] and DFe, d) CDOM representative absorption coefficients at 254 nm (colour scale) and 300 nm (contours) and e) CDOM fluorescence at 450 nm. A white contour indicates the constraining value for the TPD of *in-situ* CDOM fluorescence (0.5 a.u.). (For interpretation of the references to colour in this figure legend, the reader is referred to the web version of this article.)

Table 3
Mean values with standard deviations, number of records and extreme values for Fe speciation and CDOM spectral properties inside and outside the TPD within the surface transect (Stations 58, 64, 69, 81, 87, 91, 96, 99, 101, 117, 119, 121, 125, 130 and 134, all ≤ 200 m). Records inside the TPD are selected on the basis of *in-situ* CDOM fluorescence.

		DFe (nM)	$[L_t]$ (Eq. nM Fe)	LogK′ (mol^{-1})	$Log\alpha_{FeL}$ (mol^{-1})	[L′] (Eq. nM Fe)	$[L_t]$/DFe ratio	HS (Eq. mg/L FA)	$F_{250/450}$ (QSU)	a_{254} (nm^{-1})	a_{300} (nm^{-1})	$S_{275-295}$ (nm^{-1})
Inside TPD	Average	2.63	2.60	11.97	1.66	0.42	1.2	0.18	3.17	5.81	2.33	0.026
	SD	1.07	0.78	0.32	1.17	0.52	0.5	0.07	0.59	1.45	0.65	0.002
	N	42	35	35	35	35	35	18	35	35	35	35
	min	0.73	1.60	11.40	− 0.08	< 0.01	0.5	0.07	2.17	3.16	1.09	0.020
	max	4.42	4.13	12.65	3.45	1.78	2.3	0.32	4.08	7.83	3.26	0.032
Outside TPD	Average	0.58	1.51	12.13	2.89	0.82	2.7	0.06	1.56	2.51	0.92	0.035
	SD	0.38	0.48	0.28	0.53	0.51	1.4	0.03	0.51	1.13	0.51	0.023
	N	128	74	74	74	74	74	38	69	76	76	76
	min	0.12	0.84	11.43	0.76	< 0.01	0.9	0.01	0.72	0.52	− 0.01	0.011
	max	2.25	3.91	12.91	4.12	3.47	8.9	0.17	2.83	5.39	2.19	0.160

Table 4
2-Ligand determination for surface transect samples in Sections 1 and 2 (Stations 58, 64, 69, 81, 87, 91, 96, 99, 101, 117, 119, 121, 125, 130 and 134, all ≤ 200 m). Two samples were resolved for 2 ligand classes inside the TPD; averages, standard deviations, minimum- and maximum values are given for the 30 samples which were resolved outside of the TPD.

		$[L_t]$ 1 (Eq. nM Fe)	LogK′ 1 (mol^{-1})	$Log\alpha_{FeL}$ 1	[L′] 1 (Eq. nM Fe)	$[L_t]$ 2 (Eq. nM Fe)	LogK′ 2 (mol^{-1})	$Log\alpha_{FeL}$ 2	[L′] 2 (Eq. nM Fe)
Inside TPD	st101 b20	2.29	13.60	3.94	0.22	1.26	11.76	2.81	1.11
	st87 b23	1.58	13.30	3.25	0.09	2.76	11.60	2.92	2.07
Outside TPD	Average	0.69	13.26	3.24	0.22	1.34	11.20	2.27	1.24
	SD	0.27	0.71	0.83	0.18	0.56	0.17	0.27	0.56
	N	30	30	30	30	30	30	30	30
	min	0.30	12.33	1.97	< 0.01	0.61	10.88	1.81	0.57
	max	1.29	15.56	6.25	0.69	3.23	11.51	2.88	3.08

resolve two ligand classes was highly biased towards samples outside the TPD where 30 samples could be resolved, as opposed to only 2 samples inside the TPD. The mean L_1 class concentration outside the TPD was 0.69 Eq. nM Fe ($0.30 \leq [L_1] \leq 1.28$, SD = 0.27), the mean L_2 class concentration was 1.34 Eq. nM Fe ($0.61 \leq [L_2] \leq 3.23$, SD = 0.56). For the same records LogK′ were 13.26 mol^{-1} (SD = 0.71) and 11.20 mol^{-1} (SD = 0.17), respectively. Inside the TPD at station 87 L_1 and L_2 concentrations were 1.58 and 2.76 Eq. nM Fe with LogK′ of 13.30 and 11.60, respectively (16 m depth). At Station 101 L_1 and L_2 concentrations were 2.29 and 1.26 Eq. nM Fe with LogK′ of 13.60 and 11.76, respectively. Depth for the Station 101 measurement was 52 m, corresponding to maxima in DFe, $[L_t]$ and CDOM at that station.

Absorption coefficients were higher in the upper 100 m for both a_{254} (Fig. 6d, colours) and a_{300} (Fig. 6d, contours) with highest values in agreement with *in-situ* CDOM fluorescence (5.81 ± 1.45 m^{-1} and 2.33 ± 0.65 m^{-1}, respectively; Table 3). Spectral slopes were slightly steeper outside of the TPD with a mean slope ratio of 0.97 ± 0.33 inside the TPD and 1.15 ± 0.63 outside the TPD. Measurements of FDOM were in agreement with a_{254} and a_{300} with $F_{250/450}$ giving high values of up to 4.08 QSU (17 m depth, Station 91) within TPD constraints against a low and relatively uniform background of 0.67 QSU (deep values, SD = 0.04 QSU, N = 65, range of 0.54 to 0.74).

Humic substance concentration [HS] profiles for the top 150 m (Fig. 7) had elevated concentrations in the upper 100 m. At Stations 87, 99, 119 and 125, which fall within TPD constraints, concentrations were higher with [HS] up to 0.32 Eq. mg/L FA (Station 99, 17.2 m). In contrast, concentrations outside the TPD (Stations 101, 117 and 134) were 0.07 Eq. mg/L FA on average (< 100 m depth, SD = 0.03 mg/L, N = 21). Overall, concentrations inside the TPD were higher with a mean of 0.14 Eq. mg/L FA against a 0.06 Eq. mg/L FA background (Table 3). In all cases, deeper values approached zero near 150 m depth.

3.4. Barents Sea properties of DFe and Fe-binding organic ligands

Dissolved Fe in the Barents Sea (Fig. 8a) was depleted at the surface and increased with depth, to a maximum concentration of 1.41 nM (414 m depth, Station 153). This is higher than most deep maxima in the other sections but lower than maxima observed at the surface in the TPD. An exception is Station 4 near Svalbard, which had a subsurface high DFe of 3.21 nM at 48 m. Mean $[L_t]$ concentration across the section is 1.43 Eq. nM Fe (SD = 0.34, N = 28; Fig. 8B). The profile at Station 4 again stands out with a subsurface maximum (2.15 Eq. nM Fe at 48 m) and a decrease in concentrations at greater depths. This was also the only station where the ratio $[L_t]$/DFe (Fig. 8C) was lower than 1 at this same depth (0.7 at 48 m). Otherwise, ratios are > 1 with values for stations 4 and 173 relatively lower compared to stations 153 and 161. Finally, LogK′ values are very constant along this section as well, similar to Sections 1 and 2 with a mean 12.13 mol^{-1} (SD = 0.28 mol^{-1}, N = 20, $11.66 \leq$ LogK′ ≤ 12.95 mol^{-1}).

4. Discussion

4.1. Deep water properties of Fe-binding organic ligands

The DFe depth profiles (Fig. 4) of the Nansen basin stations have a traditional nutrient-like profile. Station 32 is the only station showing a subsurface maximum coupled with surface depletion, as well as an increase towards the sea floor. This subsurface maximum coincided with the strongest AAW influence observed over the Nansen basin (Fig. 2) and was only observed near the continental shelf. Klunder et al. (2012b) observed high DFe values at 400 m, 1000 m and near the bottom over the Barents Sea slope at stations with approximately the same location as our Station 32. While our data had a less variable character, our vertical resolution was lower. The occurrence of a maximum at that study's slope station at 400 m was explained by melt water influence while the 1000 m and bottom maxima were connected to a slope influence. Our data for Station 32 shows a maximum from 200 to 500 m. However, attenuation data representing turbidity (not shown) did not show an increase coinciding with increased DFe at our Station 32. It is possible that our sampling location was less acutely at the slope, limiting slope resuspension effects. With the data available to

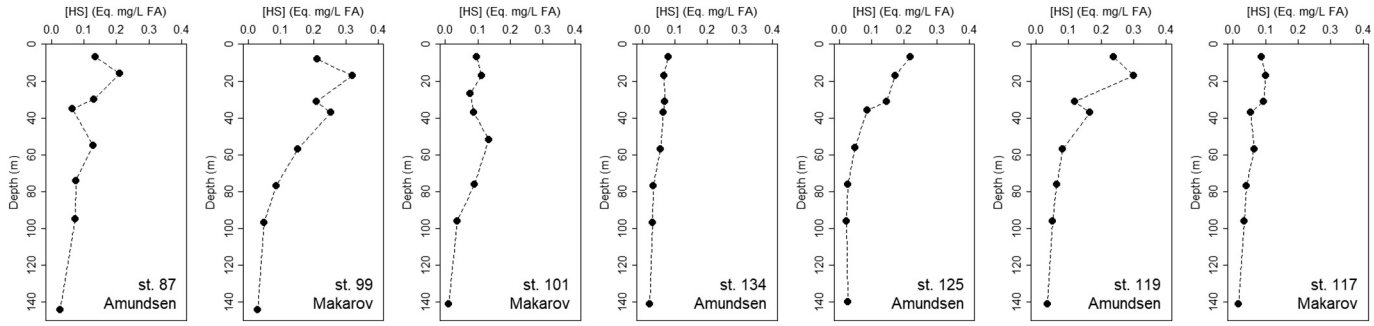

Fig. 7. Depth profiles of humic substances of stations in Sections 1 and 2 of the upper 150 m expressed in equivalent mg/L of FA. Stations and basins where these were sampled are indicated.

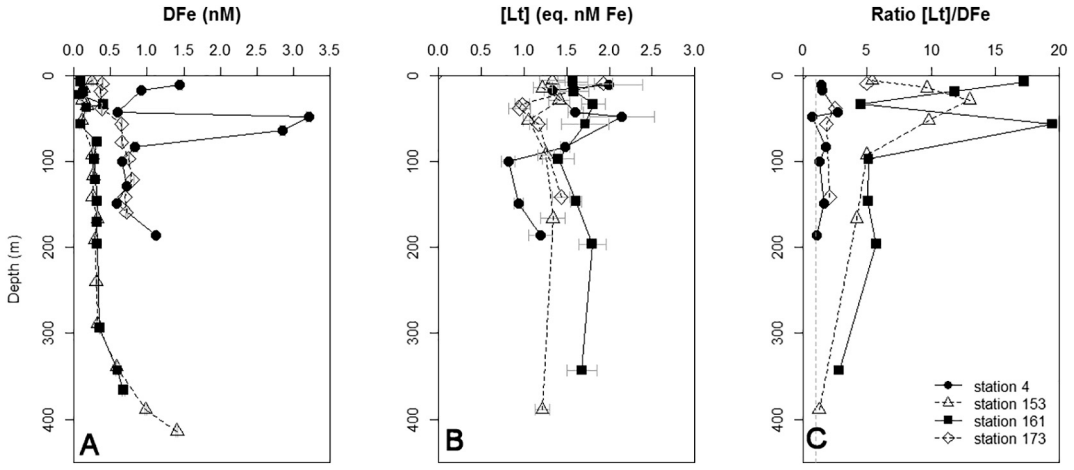

Fig. 8. Depth profiles of DFe and organic ligand characteristics of Stations 4, 153, 161 and 173 along Section 3 in the Barents Sea. A) DFe in nM, B) [L_t] in Eq. nM Fe and C) the ratio between [L_t] and DFe. The dashed line indicates a ratio of 1.

us the distinction cannot be made if the Station 32 DFe increases were due to an Atlantic influence, meltwater or slope resuspension influence.

Overall, DFe at depths over 200 m was not influenced significantly by location and, where DFe was enriched in the upper 200 m, did not differ beyond standard deviations between deep water masses. Only in the Makarov basin did DFe gradually decrease with depth (Fig. 4), which has earlier been attributed to scavenging (Thuróczy et al., 2011; Klunder et al., 2012b). Klunder et al. (2012b) conclude the lower deep DFe concentrations in the Makarov Basin may be attributed to the scavenging removal in the Makarov Basin being particularly more effective due to a longer water mass residence time than in the other basins, allowing for a longer exposure to the scavenging process and due to lower input from hydrothermal sources. This in turn was coupled with a lower ligand binding strength found in the Makarov and Amundsen Basins (Thuróczy et al., 2011). However, in the present study we could not replicate such a clear difference between LogK′ in the Nansen, Amundsen and Makarov basins, with mean values of 12.08, 11.93 and 12.11, respectively (> 1000 m depth; SD's of 0.39, 0.22 and 0.31 for N of 7, 21 and 8, respectively, Table 1). On the contrary, the LogK′ values were very similar across the dataset. At depths over 200 m, [L_t] showed little variability with average concentrations of 1.35, 1.37 and 1.20 Eq. nM Fe in the Nansen, Amundsen and Makarov basins, respectively (SD = 0.30, 0.28 and 0.21 Eq. nM Fe, N = 13, 31 and 19).

For those samples where two ligand classes could be resolved, L_1 and L_2 did not significantly differ between basins. Although the determination could not be made in all samples, the spread and deviations between L_1 and L_2 as well as their corresponding LogK′ values were very small, indicating the good quality of the data. One notable difference between basins was a slight increase in [L_t] with depth in the Makarov basin stations (96, 99, 101 and 134; Fig. 4). This was more pronounced in the ratio [L_t]/DFe (Fig. 5) as first described by (Thuróczy et al., 2011). This, coupled with a higher particulate Fe concentration at depth in that study, further confirmed the aforementioned stronger effect of scavenging in the Makarov Basin. In the present study, surface (< 200 m depth) [L_t] was clearly enriched, further discussed in greater spatial resolution in the next section. Surface ratios of [L_t]/DFe between 0 and 1 suggest that further Fe input would tend to precipitate, possibly adding to a higher scavenging influence lower in the water column. A strong surface influence of humic substances, which would increase the [L_t]/DFe ratio, would preclude such surface precipitation as an explanation, though a higher particle load might explain increased scavenging. However, attenuation data from rosette sampler sensors in the Makarov Basin do not support increased particle loads. While humic substances have in some cases been reported at depth (Laglera and van den Berg, 2009), persistence lower in the water column or flocculation of these high-MW substances and/or possible contributions to the scavenging effects are not known. Additionally, the presence of a similar riverine surface influence over part of the Amundsen basin did not lead to increased scavenging effects at depth at those stations. Values for Logα_{FeL} also did not change significantly with depth in the Makarov basin, indicating that the reactivity of the ligands present there did not change with depth. Our findings confirm that DFe input and water mass differences in the deep Makarov basin drive Fe speciation there (Thuróczy et al., 2011; Klunder et al., 2012b), as there were no indications of fluxes in Fe binding organic ligands.

4.2. Surface properties of DFe, Fe-binding organic ligands, CDOM and humic substances

The TPD influence area was constrained using *in-situ* CDOM fluorescence data. While this sensor was uncalibrated, its agreement with other CDOM spectral properties was excellent. As the sensor was on the

rosette sampler, typically preceding UCC casts, it was initially used to target UCC sampling for Fe-binding ligand and CDOM. Additionally, any calibration performed would depend on a standard that may not be representative of the study area, as further discussed later in this section, yielding a similarly arbitrary relation. Average DFe inside the TPD was significantly higher at 2.63 nM (SD = 1.07 nM, N = 42) against an average background outside the TPD of 0.58 nM (SD = 0.38 nM, N = 127, Table 3). In concert, average [L_t] inside the TPD was higher than outside with hardly any overlap in standard deviations at 2.60 Eq. nM Fe (SD = 0.78 Eq. nM Fe, N = 35) and 1.51 Eq. nM Fe (SD = 0.48 Eq. nM Fe, N = 74). Note that the average [L_t] inside the TPD was actually slightly lower than DFe. Where this was the case in specific records, assuming that DFe beyond the inorganic solubility of Fe in seawater (Liu and Millero, 2002) must be bound to organic ligands (Gledhill and van den Berg, 1994), DFe being higher than [L_t] indicates that more ligands were present in these locations than measured with the TAC method and the analytical window used in this study. The [L_t]/DFe ratio, where this is between 0 and 1, also indicates insufficient Fe binding capability to explain DFe (Fig. 6c). Average [L_t]/DFe ratios inside the TPD were 1.2 (SD = 0.5, N = 35) with a minimum ratio of 0.5 (Table 3). The [L_t]/DFe ratio outside the TPD was much higher with an average value of 2.7 (SD = 1.4, N = 74), indicating a surplus of ligands detected with the TAC method. Further differences between ligands inside and outside the TPD are shown by low [L′] (Fig. 6b). Low [L′] indicates ligand saturation, which coincided with highest DFe and [L_t] in the surface transect. LogK′ values were similar inside and outside the TPD ($11.97 \pm 0.32\ mol^{-1}$ and $12.13 \pm 0.28\ mol^{-1}$, respectively; Table 3). This suggests all ligands were of similar strength, though measured within the confines of the binding strengths our competitive exchange ligand TAC will establish an equilibrium with.

Two ligand classes could only be resolved for samples outside the TPD barring two exceptions (Table 4). The corresponding LogK′ values did not significantly differ from those found for the two ligand classes found in > 200 m samples, much like in the case of the single ligand class determination. The inability to detect two ligand classes in samples inside the TPD is not surprising given that ligands inside the TPD were found to be near saturation, as determined from the [L_t]/DFe ratio nearing 1 and low [L′]. In such a case a stronger ligand class would be entirely saturated and therefore undetectable through titration with TAC at the detection window used in this study. The observed lack of significant difference in LogK′ inside and outside the TPD therefore may also be attributed to measurements using TAC only showing part of the riverine input effect on speciation. To what extent an alternate added ligand might alleviate this must be attempted, perhaps only a combination of analytical methods provides a full understanding in this study area. The high variability of Logα_{FeL} inside the TPD is also explained by the highly saturated state of ligands there. As α_{FeL} is the product of [L′] and K′, when [L′] nears 0 the value of Logα_{FeL} is no longer representative of the true reactivity of the ligands. While less precise at saturation, Logα_{FeL} may be more descriptive of the situation as the ratio [L_t]/DFe simply approaches 1 and [L′] approaches 0 asymptotically, while Logα_{FeL} amplifies the differences and adds information on the probability of Fe binding (Gledhill and Gerringa, 2017).

According to Laglera et al. (2011) the method we use to determine the ligand characteristics applying TAC as competing ligand is not capable of measuring the entire contribution of humic substances to the ligand pool. The many weaker binding sites in a humic substance may not fall within the typically employed detection windows for TAC. While applying a lower analytical window for TAC increased the detectability of weaker ligands (Gerringa et al., 2007), fulvic acid additions could not be detected, confirming at least a part of Laglera's conclusions. According to Laglera et al. (2011), TAC itself interacts with humic substances, suppressing Fe-TAC complexation. Indeed, adding the IHSS FA standard to a sample did not significantly change [L_t] and LogK′ determinations (unpublished results; addition of 0.1 mg/L FA to Station 134 sample from 2695 m depth).

From earlier studies using TAC, riverine influence on the ligand pool was found in a number of occasions (*e.g.*Gerringa et al., 2007; Batchelli et al., 2010), including the influence of Arctic outflow water on surface Fe speciation in the Western Atlantic Ocean (Gerringa et al., 2015) but this riverine input of ligands is probably underestimated given that part of the humic influence is missing. Other studies concentrating on the effect of humic substances in particular apply other methods such as 2,3-dihydroxynaphtalene (DHN) and salicylaldoxime (SA) (Laglera and van den Berg, 2009; Abualhaija et al., 2015; Mahmood et al., 2015). Prior intercomparisons between the TAC and SA methods showed that agreement within similar detection windows could be dependent on the sample matrix. A study in the North Pacific comparing methods concluded that methods using TAC and SA gave more or less comparable results but still recommended further research (Buck et al., 2012). A comparison study in the north Atlantic showed very good agreement between the methods using SA and TAC when the 1-ligand model was applied to the data. However, when applying the 2-ligand model to the two datasets different results were obtained, with the SA method resulting in the discrimination of 2 ligands where the TAC method could not (Buck et al., 2016). While an increased Fe-binding organic ligand concentration inside the TPD is indicated in the present study, the exact effect on speciation might be underestimated by the analytical method employed here.

CDOM spectral properties a_{254} and a_{300} represent CDOM concentrations, and therefore the organic substance load also including humic substances (Helms et al., 2008). $F_{250/450}$ is typically reported as humic-like substances (Coble, 2007). All these properties had very good agreement with our *in-situ* CDOM fluorescence discriminator for the TPD (Fig. 3d; Fig. 6, white contours). As a result, significantly higher average values were recorded inside the TPD for all three terms (Table 3). The spectral slope at an interval of 275–295 nm ($S_{275–295}$) showed more uniformly low slopes inside the TPD compared to outside the TPD (0.026 *vs.* $0.035\ nm^{-1}$, SD = 0.002 and $0.023\ nm^{-1}$, respectively) which, coupled with high absorbance at both 254 and 300 nm, indicate a higher CDOM concentration of samples inside the TPD (Helms et al., 2008). However, higher-wavelength intervals fall outside of our instrument's sensitivity, with $S_{350–400}$ at or below the limit of detection for many samples (N = 62 for $S_{350–400}$*vs.* N = 76 for $S_{275–295}$ for outside-TPD samples), creating a bias in the dataset for samples with higher absorbance, and therefore, slope ratios yielded little further information. In most oceanic samples, slope ratios are driven by the UV slope ($S_{275–295}$; Helms et al., 2008) and given the restrictions of our equipment our discussion is focused on these properties.

Measurements of [HS] inside the TPD yielded a higher average of 0.18 Eq. mg/L FA (SD = 0.07 Eq. mg/L FA, N = 18) against an average 0.06 Eq. mg/L FA outside the TPD (SD = 0.03 Eq. mg/L FA, N = 38). From the [HS] profiles (Fig. 7) it is visually apparent that inside-TPD stations (87, 99, 119 and 125) had well-defined surface enrichment. In prior studies measuring riverine-sourced humic substances it was shown that humic substance concentrations explained 100% of Fe-binding organic ligands measured (Laglera and van den Berg, 2009; Abualhaija et al., 2015). According to Laglera and van den Berg (2009) 1 mg/L Suwannee River FA should offer an Fe binding capacity of 16.7 ± 2.0 nM under controlled purified circumstances using UV digested seawater. By extension, the 0.18 Eq. mg/L FA found in the present study would account for an Fe binding capacity of around 3.0 ± 0.4 nM. Inside the TPD, [L_t] was shy of that at 2.60 ± 0.78 nM (Table 3). However, while it is evident from literature and our own findings that the TAC method cannot measure all humic substance influence, the [L_t] we found did not differ from the humic contribution we measured outside of standard deviation. Furthermore, [L_t] increase from deep to surface is more pronounced in Section 1 than it is in Section 2 (Fig. 6b). With a DFe increase of similar proportion in either section (Fig. 6a), this leads to a stronger effect of low (between 0 and 1) ratios of [L_t] and DFe, indicating a lack of ligands to explain DFe concentrations in Section 2. This may indicate a stronger

Table 5
Spearman rank order correlations of Fe speciation properties with [HS] and CDOM spectral properties in the surface transect. All p-values < 0.001.

	[HS]	F_{450}	a_{254}	a_{300}	$S_{275–295}$
DFe	0.90	0.93	0.90	0.87	− 0.52
[L_t]	0.69	0.74	0.69	0.66	− 0.36
[L′]	− 0.47	− 0.50	− 0.53	− 0.54	0.36
Ratio [L_t]/DFe	− 0.79	− 0.83	− 0.82	− 0.80	0.49

underestimation of ligands in Section 2 than in Section 1, and an overestimation when compared to [HS] in Section 1. The differences between Sections 1 and 2 are not surprising as the TPD has a transition time of 3 years (Gregor et al., 1998) and the TPD flow path varies yearly with the arctic oscillation (Macdonald et al., 2005). Therefore, local samples from the TPD are subject to changes in conditions over time in the source catchments, sea ice melt and coverage and shelf sea interaction. Additionally, possible modification of the surface water influence over time may take place, *e.g.* by microbial action, local DOM production, deposition by ice rafted sediments, *etc*.

Many of these processes may be presumed involved in the local CDOM pool and contributing to the ligand pool regardless of transition time. Ice rafted sediments have been indicated to carry trace elements (Hölemann et al., 1999) and presumably Fe-binding organic ligands. Occasionally we found areas of strong discolouration by ice rafted sediments during the PS94 expedition (2 sampling locations pending analysis, cruise report: Schauer, 2016), but this remained a local phenomenon. Biota may also have been present to release DOM. However, given that all stations in Sections 1 and 2 were under full ice cover at the time of sampling, contemporaneous microbial activity may be presumed to be minimal. EPS carried by the TPD from the ostensibly more active source areas may be a factor, given that recalcitrant fractions are known to be present (Hofmann et al., 2009). However, the relative contribution thereof cannot be ascertained as EPS are methodically indistinguishable from HS using the method here employed (Hassler et al., 2011b).

It must be noted that [HS] were measured in equivalent [FA] using the IHSS Suwannee River standard. This is a humic substance originating in the Okefenokee Swamp in GA, USA, depositing in the blackwater Suwannee River which ultimately flows out in the Gulf of Mexico. This FA standard may not necessarily represent humic substances present in the Arctic Ocean, which for our study area originate from broad Arctic shelves, sea ice, and rivers with catchments characterized by permafrost soil under pressure of climate change (Schuur et al., 2015). How measurement of humic substances from this area would differ electrochemically is currently unknown as there is no representative standard available for this type of catchment. However, changes in riverine discharge as a result of changing conditions, both quantitatively and qualitatively, have been described (Peterson et al., 2002; Vonk et al., 2012, 2013). Finally, particle load from rivers is also high, potentially transporting particle- or colloid-bound Fe into the Arctic Ocean interior (Hirst et al., 2017). Particles and colloids may contribute to the dissolved Fe pool *via* exchange with ligand-bound DFe, as is also found to be the case in the Southern Ocean (von der Heyden et al., 2012). The exchangeability of particle- or colloid-bound DFe in the Arctic Ocean is not certain, given the unknown extent to which these are refractory (Thuróczy et al., 2011). If there is a large fraction of irreversibly bound DFe, [L_t] will be overestimated (Gledhill and Buck, 2012; Gerringa et al., 2014). Particle-bound Fe may be a source of exchangeable DFe and of binding sites, procedurally put outside of the methodological size cut-off due to filtration.

CDOM (a_{254}, a_{300}; Fig. 6d) and FDOM ($F_{250/450}$, Fig. 6e) spectral properties also showed higher values in Section 1, while [HS] profiles suggest that surface concentration increases were similar at stations inside the TPD in either transect (Stations 87 and 99 in Section 1, Stations 119 and 125 in Section 2; Fig. 7). This suggests that the CDOM spectral properties measured here are also limited in their ability to elucidate the relative contribution of humic substances. The most specific humic-like descriptors for CDOM are reported to be slope ratios (Helms et al., 2008) and comprehensive analysis of Excitation Emission Matrix fluorescence spectroscopy (EEM, Walker et al., 2009). Comprehensive analysis of absorption spectra also shows promise in deriving source information from DOM (Reader et al., 2015), but has not yet been applied in this region. More detailed exploration of CDOM spectral properties using EEMs in concert with absorption spectra and using a more sensitive instrument may improve upon these comparisons, allowing for the use of multivariate analysis to explore of humic-like substances (Reader et al., unpublished data).

In order to further explore the relation between ligand characteristics on one hand and CDOM spectral properties and [HS] on the other hand, pairwise Spearman rank-order correlations were performed on the surface transect data (≤ 200 m depth, Stations 58 to 101 and 117 to 134). These are summarized in Table 5 where these are reported for DFe, [L_t] and their ratio and [L′]. There was a strong correlation of [HS] with DFe. However, while a reasonable correlation with [L_t] existed, it is less pronounced. This may be explained by the specific FA standard for [HS] used, which may not represent local humic substances. Additionally, the inherent non-specificity of CLE-AdCSV methods and the competitive ligand TAC's reported inability to measure all humic substances (Laglera et al., 2011) may limit to what extent [L_t] is explained by [HS]. Similarly, correlations between DFe and $F_{250/450}$, a_{254} and a_{300} were strong and those for [L_t] and [L′] were less pronounced. Correlations of these humic indicators with the ratio [L_t]/DFe was higher again, indicating that the fact we measured insufficient ligands to explain DFe inside the TPD has good agreement with [HS]. Correlations between the spectral slope ($S_{275–295}$) and [L_t], [L′] and the ratio [Lt]/DFe in a similar fashion as above were less pronounced. However, correlations for S_{350} (not shown) could not be resolved, and therefore nor could the slope ratio. As the variability of LogK′ is very low across the dataset, no correlation statistics were calculated for it.

Spectral properties of CDOM are not available for the Barents Sea transect. Values for [L_t] and the ratio [L_t]/DFe differed from measurements in the surface Arctic Ocean. Dissolved Fe concentrations were depleted at the surface here, while [L_t] had a well-mixed character to depths beyond 200 m. The ratio [L_t]/DFe was low but not saturated at nearshore Stations 4 and 173, while it was high at the surface with a decline with depth in the central Barents Sea stations (153 and 161). This shows that the riverine influence inside the TPD was different to that of this shelf sea in terms of Fe-binding organic ligands. The Barents Sea is characterized by a large influence of Atlantic water and the continental shelf, and lacks the influence of large rivers and organic loads from such catchments (Rudels, 2012).

Finally, we may estimate the TPD flow path by way of the tracers we have measured, particularly DFe, CDOM spectral properties a_{254}, a_{300} and $F_{250/450}$, and to a lesser extent [L_t], [L′] and the ratio [L_t]/DFe. While [HS] confirmed this information, the horizontal resolution for these measurements was insufficient to indicate the TPD flow path directly. Hydrographical data supports the fundamentally different character of the surface water, particularly in terms of density. However, a distinction in ice melt and river water cannot be made based on our data, but other data collected during the cruise will help elucidate this distinction. In synthesis, we can surmise that Stations 81 to 99 in Section 1 and Stations 119 to 130 in Section 2 are part of the TPD. While Stations 101 and 117 fall outside of our initial constraint of the TPD using the *in-situ* CDOM fluorescence, some influence of the TPD is apparent here and therefore the border of the flow path is not sharply defined. The indication of the TPD flow path in Fig. 1 is based on the preceding.

5. Conclusions

Nearly invariant LogK′ was found across the entire dataset, indicating a single group of ligands or very consistent mix of ligands in terms of binding strength. Two ligand groups could be resolved for part of the dataset, and where these could be resolved the LogK′ values were again very consistent across basins. Scavenging seemed relatively important in the deeper Makarov basin, and low Fe in deep Makarov is most probably driven by DFe sources alone, confirming earlier findings. In the surface Arctic Ocean Fe-binding organic ligands correlated significantly with CDOM, including humic proxies, which in turn tie this to the TPD. A lack of ligands to explain DFe indicated by $[L_t]$/DFe ratios < 1 was unexpected, but agree with an underestimation by the TAC method in detecting humic influences or DFe contributors beyond the scope of our measurements. While average ligand concentrations measured inside the TPD agreed with [HS] found within standard deviations, similar LogK′ were found inside and outside of the TPD. A differing response in relation to the distance from the TPD source area of Sections 1 and 2 suggests that modification during surface transport across the Arctic Ocean surface and/or seasonal differences are present. Elucidating the role of humics specifically, beyond the correlation indicated in this study, requires a different approach in CLE-AdCSV. Different methods have their place in a detailed analysis of Fe-binding organic ligands. Such measurements may then be coupled with high resolution direct measurement of humic substances, which call for a more representative expression standard for the catchments around the influential mediterranean Arctic. Detailed examination of CDOM pools and their characteristics, along with other tracers, may enhance our understanding of riverine influences further.

The TPD flow path was well-discernible from our measurements of known tracers such as CDOM spectral properties and DFe, sustained by $[L_t]$. DFe and $[L_t]$ inside the TPD flow path were high. The TPD and therefore the Arctic major rivers are a source of Fe-binding organic ligands. River output of CDOM is already known to be under the influence of climate change, possibly changing Fe speciation throughout the Arctic Ocean surface. As waters from the Arctic Ocean flow out into the Atlantic Ocean through the Fram strait, the effect of climatic change in Arctic river catchments and sea ice dynamics may reach well beyond the Arctic Circle.

Acknowledgements

We would like to thank captain Schwarze and the crew of FS Polarstern on expedition PS94, as well as the Alfred Wegener Institute for logistical support. We are indebted to Ursula Schauer who served as PI during the cruise, hearing and facilitating the many requests of the diverse groups, balancing requests to great satisfaction of all. Benjamin Rabe is recognized for providing the hydrographical dataset for the cruise. NIOZ supported the expedition with logistics and instrumentation, as well as provided the facilities for the many analyses at the home lab. We thank Jan van Ooijen for his nutrient analyses on board. Aridane Gonzalez, Lars-Eric Heimburger and Michael Staubwasser are recognized for their assistance in trace metal clean sampling, Sven Ober for the operation and maintenance of the PRISTINE sampling system. Discussions with Luis Laglera were invaluable for our measurement of humic substances during the expedition and students David Amptmeijer and Robert Sluijter have performed many measurements in the home lab. The helpful comments of Corina Brussaard have greatly benefited this manuscript. Our participation in this GEOTRACES expedition was funded by NWO under contract number 822.01.018 to L.J.A. Gerringa.

References

Abualhaija, M.M., Whitby, H., van den Berg, C.M.G., 2015. Competition between copper and iron for humic ligands in estuarine waters. Mar. Chem. 172, 46–56.
Amon, R.M.W., Gereon, B., Benedikt, M., 2003. Dissolved organic carbon distribution and origin in the Nordic Seas: exchanges with the Arctic Ocean and the North Atlantic. J. Geophys. Res. 108, 3221.
Batchelli, S., Muller, F.L.L., Chang, K.C., Lee, C.L., 2010. Evidence for strong but dynamic iron-humic colloidal associations in humic-rich coastal waters. Environ. Sci. Technol. 44, 8485–8490.
Bauch, D., Cherniavskaia, E., Timokhov, L., 2016. Shelf basin exchange along the Siberian continental margin: modification of Atlantic water and lower halocline water. Deep-Sea Res. I Oceanogr. Res. Pap. 115, 188–198.
Buck, K.N., Moffett, J., Barbeau, K.A., Bundy, R.M., Kondo, Y., Wu, J., 2012. The organic complexation of iron and copper: an intercomparison of competitive ligand exchange–adsorptive cathodic stripping voltammetry (CLE-ACSV) techniques. Limnol. Oceanogr. Methods 10, 496–515.
Buck, K.N., Gerringa, L.J.A., Rijkenberg, M.J.A., 2016. An intercomparison of dissolved iron speciation at the Bermuda Atlantic Time-series Study (BATS) site: results from GEOTRACES Crossover Station A. Front. Mar. Sci. 3, 262.
Butler, A., 2005. Marine siderophores and microbial iron mobilization. Biometals 18, 369–374.
Coble, P.G., 2007. Marine optical biogeochemistry: the chemistry of ocean color. Chem. Rev. 107, 402–418.
Coble, P.G., Del Castillo, C.E., Avril, B., 1998. Distribution and optical properties of CDOM in the Arabian Sea during the 1995 Southwest Monsoon. Deep-Sea Res. II Top. Stud. Oceanogr. 45, 2195–2223.
Cooper, L.W., Whitledge, T.E., Grebmeier, J.M., Weingartner, T., 1997. The nutrient, salinity, and stable oxygen isotope composition of Bering and Chukchi Sea waters. J. Geophys. Res. 102, 12563–12573.
Croot, P.L., Johansson, M., 2000. Determination of iron speciation by cathodic stripping voltammetry in seawater using the competing ligand 2-(2-thiazolylazo)-p-cresol (TAC). Electroanalysis 12, 565–576.
Cuttler, G., Andersson, P.S., Codispoti, L.A., Croot, P.L., Francois, R., Lohan, M.C., Obata, H., Rutgers van der Loeff, M., 2010. Sampling and Sample-handling Protocols for GEOTRACES Cruises. pp. 1–238.
de Baar, H.J.W., Buma, A.G.J., Nolting, R.F., Cadee, G.C., Jacques, G., Treguer, P.J., 1990. On iron limitation of the Southern Ocean: experimental observations in the Weddell and Scotia Seas. Mar. Ecol. Prog. Ser. 65, 105–122.
Frey, K.E., McClelland, J.W., 2009. Impacts of permafrost degradation on arctic river biogeochemistry. Hydrol. Process. 23, 169–182.
Geider, R.J., La Roche, J., 1994. The role of iron in phytoplankton photosynthesis, and the potential for iron-limitation of primary productivity in the sea. Photosynth. Res. 39, 275–301.
Gerringa, L.J.A., Veldhuis, M.J.W., Timmermans, K.R., Sarthou, G., de Baar, H.J.W., 2006. Co-variance of dissolved Fe-binding ligands with phytoplankton characteristics in the Canary Basin. Mar. Chem. 102, 276–290.
Gerringa, L.J.A., Rijkenberg, M.J.A., Wolterbeek, H.T., Verburg, T.G., Boye, M., de Baar, H.J.W., 2007. Kinetic study reveals weak Fe-binding ligand, which affects the solubility of Fe in the Scheldt estuary. Mar. Chem. 103, 30–45.
Gerringa, L.J.A., Rijkenberg, M.J.A., Thuróczy, C.E., Maas, L.R.M., 2014. A critical look at the calculation of the binding characteristics and concentration of iron complexing ligands in seawater with suggested improvements. Environ. Chem. 11, 114–136.
Gerringa, L.J.A., Rijkenberg, M.J.A., Schoemann, V., Laan, P., de Baar, H.J.W., 2015. Organic complexation of iron in the West Atlantic Ocean. Mar. Chem. 177, 434–446.
Gerringa, L.J.A., Rijkenberg, M.J.A., Bown, J., Margolin, A.R., Laan, P., de Baar, H.J.W., 2016. Fe-binding dissolved organic ligands in the oxic and suboxic waters of the Black Sea. Front. Mar. Sci. 3, 1–16.
Gledhill, M., Buck, K.N., 2012. The organic complexation of iron in the marine environment: a review. Front. Microbiol. 3, 69.
Gledhill, M., Gerringa, L.J.A., 2017. The effect of metal concentration on the parameters derived from complexometric titrations of trace elements in seawater—a model study. Front. Mar. Sci. 4, 254.
Gledhill, M., van den Berg, C.M.G., 1994. Determination of complexation of iron(III) with natural organic complexing ligands in seawater using cathodic stripping voltammetry. Mar. Chem. 47, 41–54.
Gordienko, P.A., Laktionov, A.F., 1969. Circulation and physics of the Arctic basin waters. In: Gordon, A.L., Baker, F.W.G. (Eds.), Oceanography: Annals of the International Geophysical Year, vol. 46. Pergamon Press, London, pp. 94–112.
Grasshoff, K., 1983. Determination of nitrate. In: Grasshoff, K., Erhardt, M., Kremling, K. (Eds.), Methods of Seawater Analysis. Verlag Chemie, pp. 143–187.
Gregor, D.J., Loeng, H., Barrie, L., 1998. The influence of physical and chemical processes on contaminant transport into and within the Arctic. In: Arctic Monitoring and Assessment Report: Arctic Pollution Issues.
Hassler, C.S., Alasonati, E., Mancuso Nichols, C.A., Slaveykova, V.I., 2011a. Exopolysaccharides produced by bacteria isolated from the pelagic Southern Ocean — role in Fe binding, chemical reactivity, and bioavailability. Mar. Chem. 123, 88–98.
Hassler, C.S., Schoemann, V., Nichols, C.M., Butler, E.C.V., Boyd, P.W., 2011b. Saccharides enhance iron bioavailability to Southern Ocean phytoplankton. Proc. Natl. Acad. Sci. U. S. A. 108, 1076–1081.
Hassler, C.S., van den Berg, C.M.G., Boyd, P.W., 2017. Toward a regional classification to provide a more inclusive examination of the ocean biogeochemistry of iron-binding ligands. Front. Mar. Sci. 4, 19.
Helms, J.R., Stubbins, A., Ritchie, J.D., Minor, E.C., Kieber, D.J., Mopper, K., 2008. Absorption spectral slopes and slope ratios as indicators of molecular weight, source, and photobleaching of chromophoric dissolved organic matter. Limnol. Oceanogr. 53, 955–969.
Hirst, C., Andersson, P.S., Shaw, S., Burke, I.T., Kutscher, L., Murphy, M.J., Maximov, T., Pokrovsky, O.S., Mörth, C.M., Porcelli, D., 2017. Characterisation of Fe-bearing particles and colloids in the Lena River basin, NE Russia. Geochim. Cosmochim. Acta

213, 553–573.
Hofmann, T., Hanlon, A.R.M., Taylor, J.D., Ball, A.S., Osborn, A.M., Underwood, G.J.C., 2009. Dynamics and compositional changes in extracellular carbohydrates in estuarine sediments during degradation. Mar. Ecol. Prog. Ser. 379, 45–58.
Hölemann, J.A., Schirmacher, M., Kassens, H., Prange, A., 1999. Geochemistry of surficial and ice-rafted sediments from the Laptev Sea (Siberia). Estuar. Coast. Shelf Sci. 49, 45–59.
IPCC, 2014. Climate Change 2014: Synthesis Report. Contribution of Working Groups I, II and III to the Fifth Assessment Report of the Intergovernmental Panel on Climate Change. IPCC, Geneva, Switzerland.
Klunder, M.B., Laan, P., Middag, R., De Baar, H.J.W., van Ooijen, J.C., De Baar, H.J.W., Van Ooijen, J.C., 2011. Dissolved iron in the Southern Ocean (Atlantic sector). Deep-Sea Res. II Top. Stud. Oceanogr. 58, 2678–2694.
Klunder, M.B., Bauch, D., Laan, P., de Baar, H.J.W., van Heuven, S., Ober, S., 2012a. Dissolved iron in the Arctic shelf seas and surface waters of the central Arctic Ocean: impact of Arctic river water and ice-melt. J. Geophys. Res. 117.
Klunder, M.B., Laan, P., Middag, R., de Baar, H.J.W., Bakker, K., 2012b. Dissolved iron in the Arctic Ocean: important role of hydrothermal sources, shelf input and scavenging removal. J. Geophys. Res. 117, C04014.
Laglera, L.M., van den Berg, C.M.G., 2009. Evidence for geochemical control of iron by humic substances in seawater. Limnol. Oceanogr. 54, 610–619.
Laglera, L.M., Battaglia, G., van den Berg, C.M.G., 2007. Determination of humic substances in natural waters by cathodic stripping voltammetry of their complexes with iron. Anal. Chim. Acta 599, 58–66.
Laglera, L.M., Battaglia, G., van den Berg, C.M.G., 2011. Effect of humic substances on the iron speciation in natural waters by CLE/CSV. Mar. Chem. 127, 134–143.
Laukert, G., Frank, M., Bauch, D., Hathorne, E.C., Rabe, B., von Appen, W.-J., Wegner, C., Zieringer, M., Kassens, H., 2017. Ocean circulation and freshwater pathways in the Arctic Mediterranean based on a combined Nd isotope, REE and oxygen isotope section across Fram Strait. Geochim. Cosmochim. Acta 202, 285–309.
Liu, X., Millero, F.J., 2002. The solubility of iron in seawater. Mar. Chem. 77, 43–54.
Macdonald, R.W., Harner, T., Fyfe, J., 2005. Recent climate change in the Arctic and its impact on contaminant pathways and interpretation of temporal trend data. Sci. Total Environ. 342, 5–86.
Mahmood, A., Abualhaija, M.M., van den Berg, C.M.G., Sander, S.G., 2015. Organic speciation of dissolved iron in estuarine and coastal waters at multiple analytical windows. Mar. Chem. 177, 706–719.
Martin, J.H., Fitzwater, S.E., Gordon, R.M., 1990. Iron deficiency limits phytoplankton growth in Antarctic waters. Glob. Biogeochem. Cycles 4, 5–12.
Mawji, E., Gledhill, M., Worsfold, P.J., Achterberg, E.P., 2008. Collision-induced dissociation of three groups of hydroxamate siderophores: ferrioxamines, ferrichromes and coprogens/fusigens. Rapid Commun. Mass Spectrom. 22, 2195–2202.
Mawji, E., Gledhill, M., Milton, J.A., Zubkov, M.V., Thompson, A., Wolff, G.A., Achterberg, E.P., 2011. Production of siderophore type chelates in Atlantic Ocean waters enriched with different carbon and nitrogen sources. Mar. Chem. 124, 90–99.
Middag, R., de Baar, H.J.W., Laan, P., Klunder, M.B., 2011. Fluvial and hydrothermal input of manganese into the Arctic Ocean. Geochim. Cosmochim. Acta 75, 2393–2408.
Millero, F.J., 1998. Solubility of Fe (III) in seawater. Earth Planet. Sci. Lett. 154, 323–329.
Mopper, K., Schultz, C.A., 1993. Fluorescence as a possible tool for studying the nature and water column distribution of DOC components. Mar. Chem. 41, 229–238.
Murphy, J., Riley, J.P., 1962. A modified single solution method for the determination of phosphate in natural waters. Anal. Chim. Acta 27, 31–36.
Netz, D.J.A., Stith, C.M., Stümpfig, M., Köpf, G., Vogel, D., Genau, H.M., Stodola, J.L., Lill, R., Burgers, P.M.J., Pierik, A.J., 2012. Eukaryotic DNA polymerases require an iron-sulfur cluster for the formation of active complexes. Nat. Chem. Biol. 8, 125–132.
Obata, H., Karatani, H., Nakayama, E., 1993. Automated determination of iron in seawater by chelating resin concentration and chemiluminescence detection. Anal. Chem. 65, 1524–1528.
Peterson, B.J., Holmes, R.M., McClelland, J.W., Vörösmarty, C.J., Lammers, R.B., Shiklomanov, A.I., Shiklomanov, I.A., Rahmstorf, S., 2002. Increasing river discharge to the Arctic Ocean. Science 298, 2171–2173.
Poorvin, L., Sander, S.G., Velasquez, I., Ibisanmi, E., LeCleir, G.R., Wilhelm, S.W., 2011. A comparison of Fe bioavailability and binding of a catecholate siderophore with virus-mediated lysates from the marine bacterium *Vibrio alginolyticus* PWH3a. J. Exp. Mar. Biol. Ecol. 399, 43–47.
Press, W.H., Teukolsky, S.A., Vetterling, W.T., Flannery, B.P., 2007. Numerical Recipes: The Art of Scientific Computing, 3rd ed. Cambridge University Press, Cambridge, United Kingdom.
R Development Core Team, 2008. R: A Language and Environment for Statistical Computing. R Foundation for Statistical Computing, Vienna, Austria.
Raiswell, R., Anderson, T.F., 2005. Reactive iron enrichment in sediments deposited beneath euxinic bottom waters: constraints on supply by shelf recycling. Geol. Soc. Lond. Spec. Publ. 248, 179–194.
Reader, H.E., Stedmon, C.A., Nielsen, N.J., Kritzberg, E.S., 2015. Mass and UV-visible spectral fingerprints of dissolved organic matter: sources and reactivity. Front. Mar. Sci. 2, 1–10.
Rijkenberg, M.J.A., de Baar, H.J.W., Bakker, K., Gerringa, L.J.A., Keijzer, E., Laan, M., Laan, P., Middag, R., Ober, S., van Ooijen, J., Ossebaar, S., van Weerlee, E.M., Smit, M.G., 2015. "PRISTINE", a new high volume sampler for ultraclean sampling of trace metals and isotopes. Mar. Chem. 177, 501–509.
Ringbom, A., Still, E., 1972. The calculation and use of a coefficients. Anal. Chim. Acta 59, 143–146.
Rudels, B., 2010. Arctic Ocean circulation. In: Steele, J., Thorpe, S., Turekian, K. (Eds.), Ocean Currents, A Derivative of the Encyclopedia of Ocean Sciences. Academic Press, pp. 647.
Rudels, B., 2012. Arctic Ocean circulation and variability - advection and external forcing encounter constraints and local processes. Ocean Sci. 8, 261–286.
Rue, E.L., Bruland, K.W., 1995. Complexation of iron(III) by natural organic ligands in the Central North Pacific as determined by a new competitive ligand equilibration/adsorptive cathodic stripping voltammetric method. Mar. Chem. 50, 117–138.
Rutgers van der Loeff, M.M., Key, R.M., Scholten, J., Bauch, D., Michel, A., 1995. 228Ra as a tracer for shelf water in the arctic ocean. Deep-Sea Res. II Top. Stud. Oceanogr. 42, 1533–1553.
Schauer, U., 2016. The expedition PS94 of the Research Vessel POLARSTERN to the central Arctic Ocean in 2015. In: Berichte zur Polar- und Meeresforsch. - Reports Polar Mar. Res. 703, pp. 170.
Schlitzer, R., 2016. Ocean Data View.
Schuur, E.A.G., Abbott, B.W., Bowden, W.B., Brovkin, V., Camill, P., Canadell, J.G., Chanton, J.P., Chapin, F.S., Christensen, T.R., Ciais, P., Crosby, B.T., Czimczik, C.I., Grosse, G., Harden, J., Hayes, D.J., Hugelius, G., Jastrow, J.D., Jones, J.B., Kleinen, T., Koven, C.D., Krinner, G., Kuhry, P., Lawrence, D.M., McGuire, A.D., Natali, S.M., O'Donnell, J.A., Ping, C.L., Riley, W.J., Rinke, A., Romanovsky, V.E., Sannel, A.B.K., Schädel, C., Schaefer, K., Sky, J., Subin, Z.M., Tarnocai, C., Turetsky, M.R., Waldrop, M.P., Walter Anthony, K.M., Wickland, K.P., Wilson, C.J., Zimov, S.A., 2013. Expert assessment of vulnerability of permafrost carbon to climate change. Clim. Chang. 119, 359–374.
Schuur, E.A.G., McGuire, A.D., Grosse, G., Harden, J.W., Hayes, D.J., Hugelius, G., Koven, C.D., Kuhry, P., 2015. Climate change and the permafrost carbon feedback. Nature 520, 171–179.
Stedmon, C.A., Markager, S., Kaas, H., 2000. Optical properties and signatures of chromophoric dissolved organic matter (CDOM) in Danish coastal waters. Estuar. Coast. Shelf Sci. 51, 267–278.
Stedmon, C.A., Amon, R.M.W., Rinehart, A.J., Walker, S.A., 2011. The supply and characteristics of colored dissolved organic matter (CDOM) in the Arctic Ocean: pan Arctic trends and differences. Mar. Chem. 124, 108–118.
Strickland, J., Parsons, T., 1972. A Practical Handbook of Seawater Analysis.
Thuróczy, C.-E., Gerringa, L.J.A., Klunder, M.B., Middag, R., Laan, P., Timmermans, K.R., de Baar, H.J.W., 2010. Speciation of Fe in the Eastern North Atlantic Ocean. Deep-Sea Res. I Oceanogr. Res. Pap. 57, 1444–1453.
Thuróczy, C.-E., Gerringa, L.J.A., Klunder, M., Laan, P., Le Guitton, M., de Baar, H.J.W., 2011. Distinct trends in the speciation of iron between the shallow shelf seas and the deep basins of the Arctic Ocean. J. Geophys. Res. 116, C10009.
van den Berg, C.M.G., 2006. Chemical speciation of iron in seawater by cathodic stripping voltammetry with dihydroxynaphthalene. Anal. Chem. 78, 156–163.
van den Berg, C.M.G., Kramer, J.R., 1979. Determination of complexing capacities of ligands in natural waters and conditional stability constants of the copper complexes by means of manganese dioxide. Anal. Chim. Acta 106, 113–120.
von der Heyden, B.P., Roychoudhury, A.N., Mtshali, T.N., Tyliszczak, T., Myneni, S.C.B., 2012. Chemically and geographically distinct solid-phase iron pools in the Southern Ocean. Science 338, 1199–1201.
Vonk, J.E., Sánchez-García, L., van Dongen, B.E., Alling, V., Kosmach, D., Charkin, A., Semiletov, I.P., Dudarev, O.V., Shakhova, N., Roos, P., Eglinton, T.I., Andersson, A., Gustafsson, Ö., 2012. Activation of old carbon by erosion of coastal and subsea permafrost in Arctic Siberia. Nature 489, 137–140.
Vonk, J.E., Mann, P.J., Davydov, S., Davydova, A., Spencer, R.G.M., Schade, J., Sobczak, W.V., Zimov, N., Zimov, S., Bulygina, E., Eglinton, T.I., Holmes, R.M., 2013. High biolability of ancient permafrost carbon upon thaw. Geophys. Res. Lett. 40, 2689–2693.
Walker, S.A., Amon, R.M.W., Stedmon, C., Duan, S., Louchouarn, P., 2009. The use of PARAFAC modeling to trace terrestrial dissolved organic matter and fingerprint water masses in coastal Canadian Arctic surface waters. J. Geophys. Res. 114, 1–12.
Zhang, C., 2014. Essential functions of iron-requiring proteins in DNA replication, repair and cell cycle control. Protein Cell 5, 750–760.